Supplementary Materials

Tissue fluidification promotes a cGAS/STING-mediated cytosolic DNA response in invasive breast cancer

Emanuela Frittoli[1,†], Andrea Palamidessi[1,†], Federica Zanardi[1], Fabio Iannelli[1,] Stefano Villa[2], Leonardo Barzaghi[1], Hind Abdo[1], Valeria Cancila[3], Galina V. Beznuskenko[1], Giulia della Chiara[1], Massimiliano Pagani[1,2], Chiara Malinverno[1], Dipanjan Bhattacharya[1], Federica Pisati[1], Weimiao Yu[4], Viviana Galimberti[5], Giuseppina Bonizzi[5], Emanuele Martini[1], Alexander Mironov[1], Ubaldo Gioia[1], Fabrizio d'Adda di Fagagna[1,6], Chiara Rossi[7], Marco Lucioni[7], Richard Tancredi[8], Paolo Pedrazzoli[8,9], Andrea Vecchione[10], , Cristiano Petrini[1], Francesco Ferrari[1,6], Chiara Lanzuolo[11], Guilherme Nader[12], Marco Foiani[1,13] , Matthieu Piel[12], Roberto Cerbino[2, ¶] , Fabio Giavazzi*[1, 2], Claudio Tripodo*[1,3] and Giorgio Scita*[1,13]

This PDF file includes:

Materials and Methods

Figs. S1 to S11

Tables S1 to S7

References (*85–112)*

Movies S1 to S9

Material and Methods

Antibodies and reagents

REAGENT or RESOURCE	SOURCE	IDENTIFIER
Antibodies		
Anti LaminB1	Abcam	Cat# ab16048
Anti LaminA/C	Santa Cruz Biotechnology	Cat# ab7292
Anti STAT2	Thermofisher	Cat# ab44-362G
Anti ISG15	Cell Signalling Technology	Cat# ab2743
Anti Vinculin	Sigma-Aldrich	Cat# abV9131
Anti RAB5A	Santa Cruz Biotechnology	Cat# ab309
Anti RAB5A	Abcam	Cat# ab109534
Anti phospho-p44/42 MAPK (ERK1/2) (Thr202/Tyr204)	Cell Signalling Technology	Cat# ab4370
Anti p44/42 MAPK (ERK1/2)	Cell Signalling Technology	Cat# ab9102
Anti p-STAT1 (58D6) (Tyr701)	Cell Signalling Technology	Cat# ab9167
Anti STAT1 (42H3)	Cell Signalling Technology	Cat# ab9175
FITC-conjugated Phalloidin	Sigma-Aldrich	Cat# P5282
Anti IRF3 (D614C)XP	Cell Signalling Technology	Cat# 11904
Anti STING/TMEM173	Novus Biologicals	Cat# NBP2-24683
Anti cGAS	Sigma-Aldrich	Cat# HPA031700
Anti IFIT1 (D2X9Z)	Cell Signalling Technology	Cat# 14769
Anti Istone H3 trimetil (Lys9)(D4W1U)	Cell Signalling Technology	Cat# 13969
Anti Istone H3 trimetil (Lys27)(C36B11)	Cell Signalling Technology	Cat# 9733
Anti fosfo γH2AX S139 (20E3)	Cell Signalling Technology	Cat# 9718
Anti-trimethyl-Histone H3 (Lys4)	Millipore	Cat#07-473
Anti-Histone H3 (acetyl K27) antibody	Abcam	Cat#4729
Anti-Histone H3 (tri methyl K9) antibody	Abcam	Cat#8898
Recombinant Anti-Histone H3 (tri methyl K9) antibody [EPR16601]	Abcam	Cat#ab176916
Anti 53BP1	Abcam	Cat# 175933
Anti p-CHK1	Abcam	Cat# ab58567
Anti α−Tubulin	Sigma-Aldrich	Cat# T5168
Anti YAP	Santa Cruz Biotechnology	Cat# 101199

Secondary Antibody (Goat Anti-Rabbit Antibody Conjugated to Horseradish Peroxidase)	Cell Signalling Technology	Cat# 7074
Secondary Antibody (Goat Anti-Mouse Antibody Conjugated to Horseradish Peroxidase)	Cell Signalling Technology	Cat# 7076
DAPI	Thermofisher	Cat# D-1306
Hoechst	Thermofisher	Cat# 62249
IncuCyte® NucLight Rapid Red dye	Sartorius	Cat# 4717
MitoTraker Red CMXRos	Thermofisher	Cat# M7512
Cy3 AffiniPure Donkey Anti-Rabbit IgG (H+L)	Jackson ImmunoResearch	Cat# 711-165-152
Cy3 AffiniPure Donkey Anti-Mouse IgG (H+L)	Jackson ImmunoResearch	Cat# 715-165-150
Donkey anti-Rabbit IgG (H+L) Highly Cross-Adsorbed Secondary Antibody, Alexa Fluor 488	Thermofisher	Cat# A32790
Donkey anti-Mouse IgG (H+L) Highly Cross-Adsorbed Secondary Antibody, Alexa Fluor 488	Thermofisher	Cat# A21202

Chemicals

Latrunculin	Thermofisher	Cat# L12370
Etoposide	Selleckchem	Cat# S1225
Docetaxel	Selleckchem	Cat# S1148
Doxycycline hyclate	Sigma-Aldrich	Cat# D9891
SYBR Gold	Thermo-Fisher	Cat# S11494
Dynasore hydrate	Sigma-Aldrich	Cat# D7693
PD0325901	Sigma-Aldrich	Cat# 444968
Blebbistatin	Sigma-Aldrich	Cat# B0560
MK-886	Sigma-Aldrich	Cat# 475889
RU.521	Selleckchem	Cat# S6841
$H^{15}1$	Selleckchem	Cat# S6652
MRT67307	Selleckchem	Cat# S7948

Critical Commercial Assays

CometAssay® Kit	Trevigen	Cat# 4250-050-K
RNeasy mini kit	Qiagen	Cat# 74104
2'3'-cGAMP ELISA Kit	Cayman Chemical	Cat# 501700
SuperScript VILO cDNA Synthesis Kit	Thermofisher	Cat#11754050

Oligonucleotides

siRNAs targeting MB21D1 (cGAS)	Horizon	Cat# L-015607-02-0010
siRNAs targeting TMEM173 (STING)	Thermofisher	Cat# s226307
siRNAs targeting IRF3	Thermofisher	Cat# s7507
siRNAs targeting IRF9	Thermofisher	Cat# s20292
siRNAs targeting STAT1	Thermofisher	Cat# s277

siRNAs targeting STAT2	Thermofisher	Cat# s13528
siRNAs targeting EZH2	Thermofisher	Cat# s4918
siRNAs targeting SUZ12	Thermofisher	Cat# s23968
siRNAs targeting TREX1	Horizon	Cat# L-013239-02-0010
siRNAs targeting YAP	Thermofisher	Cat# s20366
siRNAs targeting TAZ	Thermofisher	Cat# s13806

qRT-PCR assays

Gene name		**assay ID**
18s	Thermofisher	Hs99999901_s1
GAPDH	Thermofisher	Hs99999905_m1
GUSB	Thermofisher	Hs99999908_m1
HPRT	Thermofisher	Hs99999909_m1
RAB5A	Thermofisher	Hs00702360_s1
RAB5B	Thermofisher	Hs00161184_m1
RAB5C	Thermofisher	Hs00428044_m1
IFI27	Thermofisher	Hs01086373_g1
IFI44	Thermofisher	Hs00197427_m1
IFI44L	Thermofisher	Hs00915292_m1
IFI6	Thermofisher	Hs00242571_m1
IFIT1	Thermofisher	Hs03027069_s1
IFIT3	Thermofisher	Hs01922752_s1
ISG15	Thermofisher	Hs01921425_s1
MX2	Thermofisher	Hs01550814_m1
OASL	Thermofisher	Hs00984387_m1
MB21D1 (cGAS)	Thermofisher	Hs00403553_m1
TMEM173 (STING)	Thermofisher	Hs00736958_m1
IRF3	Thermofisher	Hs01547277_m1
IRF9	Thermofisher	Hs00196051_m1
STAT1	Thermofisher	Hs01013996_m1
STAT2	Thermofisher	Hs01013115_g1
LMNA	Thermofisher	Hs00153462_m1
LMNB1	Thermofisher	Hs01059210_m1
EZH2	Thermofisher	Hs01016789_m1
SUZ12	Thermofisher	Hs00248742_m1
CDH1	Thermofisher	Hs00170423_m1
AXIN2	Thermofisher	Hs00610344_m1
CDH2	Thermofisher	Hs00169953_m1
EGF	Thermofisher	Hs01099999_m1
MMP13	Thermofisher	Hs00942584_m1

ZEB1	Thermofisher	Hs00232783_m1
CTGF	Thermofisher	Hs00170014_m1
CYR61	Thermofisher	Hs00998500_g1
ANKRD1	Thermofisher	Hs00923602_g1
TREX1	Thermofisher	Hs03989617_s1
YAP	Thermofisher	Hs00902712_g1
TAZ	Thermofisher	Hs00179826_m1
Gapdh	Thermofisher	Mm99999915_g1
Gusb	Thermofisher	Mm01197698_m1
Hprt1	Thermofisher	Mm00446968_m1
Cxcl10	Thermofisher	Mm00445235_m1
Ifi35	Thermofisher	Mm01260550_g1
Ifit1	Thermofisher	Mm00515153_m1
Irf7	Thermofisher	Mm00516793_g1
Irf9	Thermofisher	Mm00492679_m1
Isg15	Thermofisher	Mm01705338_s1
Oas3	Thermofisher	Mm00460944_m1
Stat1	Thermofisher	Mm00439531_m1
Stat2	Thermofisher	Mm00490880_m1
Rab5a	Thermofisher	Mm01278246_m1

Cell cultures and transfection

MCF10.DCIS.com cells were provided by J. F. Marshall (Barts Cancer Institute, Queen Mary University of London, UK) and maintained in DMEM/F12 (Biowest) supplemented with 5% horse serum (Life Technologies), 2 mM L-Glutamine (EuroClone), 0.5 mg/ml Hydrocortisone (Sigma-Aldrich), 10 µg/ml Human insulin (Sigma-Aldrich) and 20 ng/ml EGF (Peprotech).
MCF10A cells were a gift from J. S. Brugge (Department of Cell Biology, Harvard Medical School, Boston, USA) and were maintained in DMEM/F12 (Biowest) supplemented with 5% horse serum (Life Technologies), 2 mM L-Glutamine (EuroClone), 0.5 mg/ml Hydrocortisone (Sigma-Aldrich), 100 ng/ml cholera toxin (Sigma-Aldrich), 10 µg/ml Human insulin (Sigma-Aldrich) and 20 ng/ml EGF (Peprotech).
SUM225 CWN (Asterand) were maintained in Ham's F12 (Life Technologies) + 5% FBS (Life Technologies) + 10 mM Hepes (EuroClone) + 5 ug/ml Human Insulin (Sigma-Aldrich) + 1ug/ml Hydrocortisone (Sigma-Aldrich) + 2 mM L-Glutamine (EuroClone).
4T1 (ATCC) were maintained in RPMI 1640 (Lonza) + 10% FBS (Life Technologies) + 2 mM L-Glutamine (EuroClone).
HaCaT (ATCC) were maintained DMEM (Lonza) + 10% FBS (Life Technologies) + 2 mM L-Glutamine (EuroClone).
Phoenix-AMPHO cells (American Type Culture Collection, CRL-3213) were used as the packaging cell line for the generation of retroviral particles and cultured as recommended by the supplier.
HEK293T (BBCF-Biological Bank and Cell factory, INT, Milan) were grown in DMEM (Lonza) supplemented with 10% FBS (Life Technologies) and 2 mM L-Glutamine (EuroClone) and used as the packaging line for lentiviral vectors.
MCF10A cells were infected with pSLIK-neo-EV (empty vector, CTR) or pSLIK-neo-RAB5A lentiviruses and selected with the appropriate antibiotic to obtain stable inducible cell lines. MCF10.DCIS.com were infected with pSLIK-hygro-RAB5B, pSLIK-neo-RAB5C, pSLIK-neo-EV (empty vector, CTR) or pSLIK-neo-RAB5A lentiviruses and selected with the appropriate antibiotic to obtain stable inducible cell lines. Constitutive expression of mCherry H2B was achieved by retroviruses infection of MCF10DCIS.com cells with pBABE-

puro-mCherry-H2B vector. pLL5.0 E-Cadherin shRNA/mEcad-GFP vector was a gift from Alpha S. Yap (Division of Molecular Cell Biology, Institute for Molecular Bioscience, The University of Queensland, Australia). pTRIP-CMV-GFP-FLAG-cGAS GFP vector was from Addgene (plasmid# 86675). pTRIP-SFFV-EGFP-NLS vector was from Addgene (plasmid# 86677).
Transfections were performed using either calcium phosphate or FuGENE HD Transfection Reagent (Promega, Cat# E2311), according to the manufacturer's instructions.
All cell lines have been authenticated by cell fingerprinting and tested for mycoplasma contamination. Cells were grown at 37 °C in a humidified atmosphere with 5% CO_2.

Generation of lentiviral and retroviral particles
Packaging of lentiviruses or retroviruses was performed following standard protocols. Viral supernatants were collected and filtered through 0.45 µm filters. Cells were subjected to four cycles of infection and selected using the appropriate antibiotic: neomycin for the pSLIK-neo vector (150 µg /ml), hygromycin for the pSLIK-hygro vector (100 µg/ml) or puromycin for the pBABE vector (2 µg/ml). After several passages, stable bulk populations were selected and induced by doxycycline hyclate (2.5 µg/ml) in order to test: (1) induction efficiency by western blotting and quantitative reverse-transcription polymerase chain reaction (qRT-PCR), and (2) the homogeneity of the cell pool.

RNA interference
siRNA delivery was achieved by mixing 50 nM of specific siRNAs with Optimem and Lipofectamine RNAiMAX Transfection Reagent (Thermofisher, Cat# 13778150). The first cycle of interference (reverse transfection) was performed on cells in suspension. The day after, a second cycle of interference (forward transfection) was performed on cells in adhesion. The siRNAs used for knocking down specific genes are reported reagents' table. For each RNA interference experiment, a negative control was performed with the same amounts of scrambled siRNAs. Silencing efficiency was controlled by qRT-PCR.

Quantitative RT-PCR analysis
Quantitative RT-PCR analysis was performed as previously described[85].Total RNA was extracted using the RNeasy Mini kit and quantified by NanoDrop to assess both concentration and quality of the samples. Reverse transcription was performed using the SuperScript VILO cDNA Synthesis kit. Gene expression was analysed by using the TaqMan Gene expression Assay (Applied Biosystems). 0.1 ng of cDNA was amplified, in triplicate, in a reaction volume of 25 µl with 10 pmol of each gene-specific primer and the SYBR Green PCR MasterMix (Applied Biosystems). Real-time PCR was performed on the 14 ABI/Prism 7700 Sequence Detector System (PerkinElmer/Applied Biosystems) using a pre-PCR step of [1]0 min at 95 °C, followed by 40 cycles of 15 s at 95 °C and 60 s at 60 °C. Specificity of the amplified products was confirmed by melting curve analysis (Dissociation Curve TM; Perkin Elmer/Applied Biosystems) and by 6% PAGE. Preparations with RNA template without reverse transcription were used as negative controls. Samples were amplified with primers for each gene and different housekeeping genes. The cycle threshold Ct values were normalized to the housekeeping gene curve. PCR experiments were performed in triplicate and standard deviations calculated and displayed as error bars. List of qRT-PCR assays is reported in reagents' table.

Immunoblotting
Cells, washed twice with cold phosphate-buffered saline (PBS), were lysed in JS buffer supplemented with proteases and phosphatases inhibitors (50 mM HEPES pH 7.5, 50 mM NaCl, 1% glycerol, 1% Triton X-100, 1.5 mM $MgCl_2$; 5 mM EGTA, protease inhibitor cocktail (Roche Basel, Switzerland), 20 mM Na pyrophosphate pH 7.5, 50 mM NaF, 0.5 M $NaVO_4$ in HEPES pH 7.5 to inhibit phosphatases). Lysates were incubated on ice for 15 min and cleared by centrifugation at 13000 r.p.m. for 30 min at 4 °C. Protein concentration was quantified by the Bradford colorimetric protein assay. The same amount of protein lysates was loaded into polyacrylamide gel in 5X SDS sample buffer. Proteins were transferred onto Protran Nitrocellulose Transfer membranes (Whatman), probed with the appropriate antibodies (reported in reagents' table) and visualized with ECL western blotting detection reagents (GE Healthcare). Incubation in primary antibodies were performed for ON at 4 °C in TBS/0.1% Tween/5% milk for antibodies recognizing the total proteins or in TBS/0.1% Tween/5% bovine serum albumin (BSA) for antibodies recognizing phosphorylated proteins.

Tissue collection

Breast biopsies were collected from women undergoing mastectomy for primary breast cancer. Donors were informed before the surgery and agreed by written consent to donate tissues. The use of human material has been reviewed by European Institute of Oncology Ethical Committees (reference to UID 2152). The permit for obtaining clinical material did not include access to basic information regarding patients and their detailed medical histories are not given to the authors. Tumor biopsies were processed immediately upon receipt and cultured as described below.

Organoids' culture

Organoids were prepared exactly as described previously[86]. In short, cells freshly isolated from human breast cancer tissues listed in the table below were embedded in 10 mg/ml cold Cultrex growth factor reduced BME type 2 and 80 µL drops of BME-cell suspension were allowed to solidify on prewarmed 24-well CELLSTAR culture plates (Greiner, Cat#662102) at 37°C for 30 min. Upon completed gelation, 500 µl of BC organoid medium was added to each well and plates transferred to humidified 37°C / 5% CO_2 incubator. Medium was changed every 4 days. Live-cell imaging was done using a confocal microscope equipped with a gas incubation system for CO_2. Organoids were labeled with IncuCyte® NucLight Rapid Red dye (1: 500) for nuclei visualization.

Sample N.	TYPE	TISSUE TYPE	DIAGNOSIS	ER (%)	PGR (%)	HER2 SCORE	HER2 %	KI67 (%)
BR 25	Pathological	Breast - Left	Infiltrating duct carcinoma	60	60	Neg		4
BR 30	Pathological	Breast - Right	Infiltrating duct carcinoma	90	90	3+	90	28
BR 39	Pathological	Breast - Left	Infiltrating duct carcinoma	95	95	Neg		12
BR 40	Pathological	Breast - Right	Cribriform carcinoma	95	30	1+	15	3
BR 44	Pathological	Breast - Right	Infiltrating duct carcinoma	95	40	Neg		22

Transcriptomics analyses

Control and RAB5A-expressing monolayers MCF10A or MCF10.DCIS.com cells were seeded in six-well plates (1.5×10^6 cells per well) and cultured until a uniform monolayer had formed. Three independent biological replicas were performed for all this analysis. RAB5A expression was induced, by adding fresh complete media supplemented with 2.5 µg/ml doxycycline hyclate to cells. Comparable cell confluence was tested by taking pictures by differential interference contrast imaging using a 10× objective and counting the number of nuclei per field. After 48 h monolayers were processed for RNA extraction using TRIzol reagent (Thermo Fisher) and processed for total RNA extraction with PureLink™ RNA Mini Kit (Thermo Fisher), according to manufacturer's instructions.

For RNA-seq analysis of breast cancer patients derived organoids, matrigel droplets containing organoids were directly lysed as described above. The RNA quality was assessed by the RNA Integrity Number (RIN) value with RNA 6000 Nano kit assay (Agilent). Only samples with RIN > 8.0 were used in this study. RNA-seq libraries were constructed according to the TruSeq mRNA Stranded preparation kit (Illumina, San Diego, USA) and sequenced at HiSeq2500.

Libraries for mRNA-Seq: mRNA-seq indexed library preparation was performed starting from 500 ng of total mRNA (Illumina, TruSeq Stranded mRNA, 20020594) according to the manufacturer's instructions. Indexed libraries were quality controlled on Agilent Bioanalyzer 2100 (High Sensitivity DNA kit), quantified (Qubit dsDNA HS Assay, Q32851), normalized and pooled to perform a multiplexed sequencing run. 1% PhiX control was added to the sequencing pool, to serve as a positive run control. Sequencing was performed in PE mode (2x75nt) on an Illumina NextSeq550 platform, generating on average 50 million PE reads per sample. Experiment was performed using biological triplicates; a total of 12 samples were sequenced.

Reads were aligned to the GRCh38/hg38 assembly human reference genome using the STAR aligner[87] with default settings with the parameter --quantMode GeneCounts in order to obtain gene counts. Differential gene expression analysis was performed using the Bioconductor package DESeq2[88] that estimates variance-mean dependence in count data from high-throughput sequencing data and tests for differential expression exploiting a negative binomial distribution-based model. Preranked gene set

enrichment analysis (GSEA) for evaluating pathway enrichment in transcriptional data was carried out using the Bioconductor package fgsea[89], taking advantage of the Hallmarks, KEGG and chemical and genetic perturbations (CGP) gene sets available from the GSEA Molecular Signatures Database (http://www.gsea-msigdb.org/gsea/msigdb/collections.jsp).

Transcription factor enrichment analysis for overlap between the input set of differentially expressed genes and entries of the ChEA and ENCODE databases was performed using the Transcription Factor Enrichment Analysis tool from the X2K Web suite (https://maayanlab.cloud/X2K/) that infers upstream regulatory networks from lists of differentially expressed genes.

Chip-Seq experiments

Control or RAB5A-expressing MCF10 DCIS.com monolayers were treated with Formaldheyde (F8775 SIGMA) in a PBS-solution (final 1%) for 10 min while rocking at room temperature and quenched with 0.125 M Glycine for 5 min. Cells were washed twice with cold PBS and scraped off the plates. PBS-washed cells were transferred to 15 ml tubes and spun down at 400g at 4C. The pellet was lysed with 1X sonication lysis buffer (10 mM Tris pH 8.0, 0.25% SDS, 2 mM EDTA, plus protease inhibitors) and incubated for at least 10 min at 4°C. Lysed chromatin was sheared at the average size of 300 bp fragments using Covaris® E220 evolution ultrasonicator (settings: duty factor 20%, peak incidence power 75 Watt, cycles per burst 200, 5 minutes). Sonicated chromatin (3 mg) was incubated overnight at 4°C with 3 mg of the following histone mark antibodies: H3K9me3 ab176916, H3K9me3 ab8898. Immunocomplexes were recovered with 20 µl of pre-blocked Protein G-Dynabeads (Thermo Fisher) for 2 h, at 4°C, and washed twice with RIPA-low salt, twice with RIPA-high salt, twice with RIPA-LiCl and once with 10 mM Tris pH 8.0 and once with 1X TE, as previously reported[90]. The washed immunocomplexes were incubated with ChIP elution buffer (10 mM Tris-HCl pH 8.0, 5 mM EDTA pH 8.0, 300 mM NaCl, 0.4% SDS) supplemented with 0.8 mg/ml Proteinase K for 1 h at 55°C and overnight at 65°C, for reverse crosslinking. The immunoprecipitated DNA was then purified by Qiagen MinElute kit (Qiagen) and eluted in 22 µl EB buffer. ChIP-seq libraries were constructed with TruSeq ChIP Library Preparation Kit (Illumina), according to the manufacturer's instructions and sequenced on Illumina HiSeq2500 platform.

Libraries for ChIP-Seq: 2 ng of DNA having fragment size 350-400bp were used to syntfhesize libraries for Chromatin Immunoprecipitation profiles (Kapa HyperPrep kit; Roche KK8504, KK8727). Indexed DNA libraries were size-selected and purified (AmpureXP, Beckman, A63881), quantitated (Qubit dsDNA HS Assay, Q32851), checked for size distribution on Agilent Bioanalyzer 2100 (DNA HS kit, Agilent, 5067-4626) and normalized for pooling. 1% PhiX control was added to the sequencing pool, to serve as a positive run control. Sequencing was performed in SR mode (1x75nt) on an Illumina NextSeq550 platform, generating on average 35 million SR reads per sample. A total of 14 samples were sequenced

SAMMY-seq experiments.

Three distinct biological replicas of control and RAB5A expressing MCF10.DCIS.com monolayers were processed for chromatin fractionation as described[91], with minor adaptions. Briefly, 3 million cells were washed in PBS 1X, and extracted in 600 µl of cytoskeleton buffer (CSK: 10 mM PIPES pH 6,8; 100 mM NaCl; 1 mM EGTA; 300 mM Sucrose; 3 mM MgCl2; 1X protease Inhibitors by Roche Diagnostics; 1 mM PMSF) supplemented with 1 mM DTT and 0,5% Triton X-100. After 10 min on wheel at 4°C the cytoskeletal structure was separated from soluble proteins by centrifugation at 900g for 3' at 4°C, and the supernatant was labeled as S1 fraction. The pellets were resuspended with 600 µl of cytoskeleton buffer, put 10 min on wheel at 4°C followed by centrifugation at 900g for 3' at 4°C. Chromatin was solubilized by DNA digestion with 25U of RNase–free DNase (Turbo DNAse; Invitrogen AM2238) in 100 µl of CSK buffer for 60 min at 37°C. To stop digestion, ammonium sulphate was added in CSK buffer to a final concentration of 250 mM and, after 5' in ice samples were pelleted at 900g for 3 min at 4°C and the supernatant was labeled as S2 fraction. The pellets were resuspended with 200 µl of CSK buffer, put 10 min on wheel at 4°C followed by centrifugation at 3000g for 3 min at 4°C. The pellet was further extracted with 100 µl of CSK buffer with 2M NaCl for 5 min at 4°C, centrifuged at 2300g 3 min at 4°C and the supernatant was labeled as S3 fraction. This treatment removed the majority of histones from chromatin. The pellets were washed twice with 200 µl of CSK buffer with 2M NaCl, put 10 min on wheel at 4°C followed by centrifugation at 3000g for 3 min at 4°C., The pellets were solubilized in 100 µl of 8M urea buffer for 10 min at room temperature to remove any remaining protein component by applying highly denaturing conditions. This fraction was labeled as S4. DNA was extracted from S2, S3 and S4 fractions. All fractions were quantified and analyzed by SDS-PAGE and immunoblotting. Anti-tubulin alpha (Sigma T5168, mouse 1:10000), H3 (Abcam ab1791, rabbit 1:4000),

Beta-Actin (Santa-Cruz sc1616, rabbit 1:4000), were used as primary antibodies. HRP-conjugated secondary antibodies were revealed with the ECL chemiluminescence kit (Thermo Fisher Scientific).

After incubation 90 min at 37°C with 6 μl of RNAse cocktail (Invitrogen AM2286) followed by 150 min at 55°C with 40 mg of Proteinase K (Invitrogen, AM2548), DNA was extracted by standard phenol/chloroform extraction, precipitated and resuspended in 15μl milliQ H2O. The S2 fraction was further purified with PCR DNA Purification Kit (Qiagen, 28106). After Qubit HS DNA quantification then samples were evaluated by capillary electrophoresis (Agilent 2100 Bioanalyzer) and then sonicated with a Covaris M220 Focused-ultrasonicator using screw cap microTUBEs with the parameters: water bath 20°C, peak power 30.0, duty factor 20.0, cycle/burst 50, duration: 125 seconds for S2 and S3 fractions, 150 seconds for S4 fraction. The DNA profiles were checked again by capillary electrophoresis (Agilent 2100 Bioanalyzer).

Libraries for SAMMY-Seq: for fractions S2, S3 and S4 obtained from chromatin fractionation procedure, at least 2.5 ng DNA were used to generate an indexed library (Kapa HyperPrep kit; Roche KK8504, KK8727). Indexed DNA libraries were purified (AmpureXP, Beckman, A63881), quantitated (Qubit dsDNA HS Assay, Q32851), checked for size distribution on Agilent Bioanalyzer 2100 (DNA HS kit, Agilent, 5067-4626) and normalized for pooling. 1% PhiX control was added to the sequencing pool, to serve as a positive run control. Sequencing was performed in SR mode (1x75nt) on an Illumina NextSeq550 platform, generating at least 30 million SR reads per sample. Experiment was performed using biological triplicates; A total of 18 samples were sequenced

SAMMY-seq and ChIP-seq data analysis

Preprocessing of sequencing reads

Sequencing reads were trimmed and adapters removed by using Trimmomatic (v0.39)[92] using the following parameters for SAMMY-seq and ChIP-seq data: 2 for seed_mismatch, 30 for palindrome_threshold, 10 for simple_threshold, 3 for leading, 3 for trailing and 4:15 for sliding window and sequence minimum length threshold of 35. As clip file has been used the trimmomatic provided dataset “TruSeq3-SE.fa” (for single end). In addition, only for SAMMY-seq data, all reads were cropped to 75 bp reads length (if longer) by setting the crop option of Trimmomatic (v0.39) to 75. After trimming, the reads were aligned using BWA (v0.7.17-r1188)[93] etting –k parameter as 2 and using as reference genome the UCSC hg38 one (only canonical chromosomes have been taken into consideration). The alignment duplicates have been marked with Picard (v2.22) (http://broadinstitute.github.io/picard/) MarkDuplicates option. And then filtered using Samtools (v1.9)[94], in addition we filtered all the reads with mapping quality lower than 1, unmapped and read fails platform/vendor quality checks (-F 1540 -q 1).
Each sequencing lane has been analysed separately up to this point and then merged.

Genomic tracks for data visualization

The comparison between sequencing reads enrichment in ChIP-seq (ChIP over input control reads enrichment) or SAMMY-seq fractions comparison was performed using the SPP (v1.16.0)[95] (v3.5.2) library. The reads have been imported from the (previously filtered) bam files using the “read.bam.tags” function, then they were filtered using “remove.local.tag.anomalies” and finally the normalized log2 reads density ratio was computed using the function “get.smoothed.enrichment.mle” setting “tag.shift = 0” and “background.density.scaling = TRUE” to exclude enriched regions from the calculation of normalization scaling factor.
The comparisons between sequencing reads enrichment were graphically plot using the R (v3.5.2) library Gviz (1.26.5) setting 1000 as number of represented points (“window” parameter).

Heterochromatin domains calling

Heterochromatin (H3K9me3 enriched) domains were defined using the EDD (v1.1.19)[96] software with parameters (binsize = 200 Kb and gap penalty = 25) processing the filtered bam files obtained as described above. The “required_fraction_of_informative_bins” parameter was set to 0.98. The unalignable regions were defined with the ENCODE Unified GRCh38 Exclusion List (previously "blacklist") and downloaded from (https://www.encodeproject.org/files/ENCFF356LFX/).

Metaprofile analysis

The metaprofile analysis was performed using DeepTools (v3.4.3)[97]. The metaprofile matrix was calculated using the “computeMatrix” command of DeepTools, using as regions of interest the heterochromatin

domains obtained from CTR H3K9me3 ChIP-seq experiment (with antibody ab-176916-Abcam), as described above, and as signal the S4/S2 or the S4/S3 SAMMY-seq fractions comparisons (log2 ratios) calculated with SPP, as described above. The domains flanking regions (upstream and downstream) were defined of a size of 1 Mb and 20 Kb was chosen as bin size for each bin representing the domain ("binSize" parameter) and the target size of the domains rescaling was defined as 3 Mb. In addition, the "skipZeros" option was added to remove regions with zero reads coverage. The metaprofile matrix was represented using the "plotProfile" tool of DeepTools using as input the previously created matrix.

Immunohistochemistry on DCIS and IDC

Immunolocalization analysis of mouse and human tissues sections

Four-micrometers-thick human and mouse tissue sections were deparaffinized, rehydrated and unmasked using Novocastra Epitope Retrieval Solutions pH6 or pH9 in thermostatic bath at 98°C for 30 minutes. Subsequently, the sections were brought to room temperature and washed in PBS. After neutralization of the endogenous peroxidase with 3% H_2O_2 and Fc blocking by a specific protein block (Leica Novocastra), the samples were incubated with the following primary antibodies: RAB5A (clone EPR5438, 1:100 pH6, ab109534, Abcam), phospho-γH2AX (1:1000 pH6, ab11174, Abcam), cGAS (clone D1D3G, 1:100 pH6, #15102, Cell Signaling), pCHK1 (1:500 pH9, ab58567, Abcam).

IHC staining for cGAS was revealed using Novolink Polymer Detection Systems (Leica Novocastra) and DAB (3,3'-Diaminobenzidine, Leica Novocastra) as substrate chromogen and the slides were counterstained with Harris hematoxylin (Novocastra).

For multiple-marker immunostainings, in order to multiplex antibodies raised in the same species, Opal Multiplex IHC kit was developed. After deparaffinization, antigen retrieval in pH6 buffer was brought to a boil at 100% power, followed by 20% power for 15 minutes using microwave technology (MWT). Sections were treated with blocking buffer for 10 minutes at room temperature before primary antibody incubation. Slides were then incubated with Polymeric horseradish peroxidase-conjugated (HRP) secondary antibody for 10 minutes and the signal was visualized using Opal 520 fluorophore-conjugated tyramide signal amplification (TSA) at 1:100 dilution. The HRP catalyze covalent deposition of fluorophores around the marker of interest. The slides were again processed with the microwave treatment to strip primary/secondary antibody complex and allow the next antigen-antibody staining. Another round of staining was performed with the second primary antibody incubation, followed by Polymeric horseradish peroxidase-conjugated (HRP) secondary antibody and Opal 620 fluorophore-conjugated tyramide signal amplification (TSA) at 1:100 dilution for signal visualization. Finally, slides were again microwaved in antigen retrieval buffer and nuclei were subsequently visualized with DAPI (4',6-diamidin-2-fenilindolo). All slides were analyzed under a Zeiss Axioscope A1 microscope equipped with four fluorescence channels widefield IF. Microphotographs were collected using a Zeiss Axiocam 503 Color digital camera with the Zen 2.0 Software (Zeiss).

Quantification of γH2AX in human primary tumor samples

We used a semi-automated image analysis pipeline to quantify the location of the γH2AX expressing cells in the tumoral ductaladenocarcinoma regions. Specifically, we employed a deep learning based nuclear segmentation (Stardist)[98] to segment individual nuclei and identified the centroid positions of each nuclei in the image frame. A semi-automated analysis was used to identify the location of whole area, the core region and the outer margin of the ductaladenocarcinoma. The proper assignment of these regions was verified by a trained pathologist. In all cases, we removed the segmented nuclei with a centroid 20 pixels from the border regions of the imaging frame. We used an automated histogram-based thresholding in each frame to identify regions with high expression of γH2AX signal, above the threshold applied. We also removed isolated small spots as noise. Next, we identified the nuclei that display either a positive or weak/absent (below the arbitrary established threshold levels) γH2AX signal. For each case, we quantified the total number of nuclei, the number of nuclei with strongly positive or weak/no γH2AX signal in the tumor core, tumor surface and in the whole tumoral areas and computed the percentage of nuclei with strongly positive γH2AX signal in the core region, tumor front regions and in the whole tumor region over 9 independent cases. The whole image analysis pipeline is presented in Movie S9.

For the quantification of the percentage of RAB5A-positive displaying γH2AX positive or cGAS positive signals. After semiautomated identification the whole area, the core region and the outer margin of the ductaladenocarcinomas, as described above, the percentage of cells in the various areas expressing express high (>2 on scale from 0.1,2,3) or low l (< 2 on scale from 0.1,2,3) levels of RAB5A identified by expert pathologists and positive for either γH2AX positive or cGAS was counted.

Cell streaming assay

As previously shown[85], cells were seeded in six-well plates (1.5 × 10^6 cells per well) in complete medium and cultured until a uniform monolayer had formed. RAB5A expression was induced, where indicated, 16 h before performing the experiment by adding fresh complete media supplemented with 2.5 µg/ml doxycycline hyclate to cells. Comparable cell confluence was tested by taking pictures by differential interference contrast imaging using a 10× objective and counting the number of nuclei per field. In the cell streaming assay, the medium was refreshed before imaging began. An Olympus ScanR inverted microscope with 10× objective was used to take pictures every 5-15 min over a 24h-48h period. The assay was performed using an environmental microscope incubator set to 37 °C and 5% CO_2 perfusion. After cell induction, doxycycline hyclate was maintained in the media for the total duration of the time-lapse experiment.

For plasma membrane tension perturbation by osmotic treatments, an equal volume of hypotonic buffer (H_2O + 1 mM $CaCl_2$ + 1 mM $MgCl_2$) was added to cell monolayer before performing experiments.

3D spheroid formation assay

MCF10.DCIS.com cells were plated on ultra-low-attachment-surface six-well plates (Corning, Cat# 3471) at a density of 5 × 10^3 cells per well. Cells were grown in serum-free condition for 10 days by adding fresh culture media every 2 days. After 7 days, 2.5 µg/ml doxycycline hyclate was added to the medium to induce RAB5A expression. Doxycycline was maintained in the medium for two days and finally spheroids were collected and processed for total RNA extraction.

Mammary fat pad tumor development in NSG mice.

All animal experiments were approved by the OPBA (Organisms for the well-being of the animal) of IFOM and Cogentech. All experiments complied with national guidelines and legislation for animal experimentation. All mice were bred and maintained under specific pathogen-free conditions in our animal facilities at Cogentech Consortium at the FIRC Institute of Molecular Oncology Foundation and at the European Institute of Oncology in Milan, under the authorization from the Italian Ministry of Health (Autorizzazione N° 604-2016).

Control and RAB5A MCF10.DCIS.com were injected into female NOD.Cg-PrkdcscidIl2rgtm1Wjl/SzJ (commonly known as the NOD SCID gamma; NSG) mice as described previously[99]. Before injection, control or RAB5A-expressing MCF10.DCIS.com cells were trypsin detached, washed twice and resuspended at a final concentration of 300000 cells/13 µl PBS. The cell suspension was then mixed with 5 µl growth factor–reduced Matrigel (BD, Cat# 354263) and 2 µl Trypan blue solution and maintained on ice until injection. Aseptic conditions under a laminar flow hood were used throughout the surgical procedure. Female NSG mice, 6–9 weeks-old, were anesthetized with 2% isoflurane and injected with a 20µl cell suspension directly in the fourth mammary fad pad. Mice were fed with doxycycline hyclate 4 days after injection. Tumor growth was monitored weekly using digital calipers, and tumor volume was calculated according to the formula: L × W2/2 = mm^3. After 3 weeks, mice were anesthetized with 2% isoflurane to remove primary tumors (mastectomy). For histological evaluation, primary tumors were fixed in 4% phosphate-buffered formalin and embedded in paraffin. 3-µm sections of tumors were made and slides were counterstained with H&E and with indicated antibodies. Fragments of primary tumors were snap frozen on dry ice and stored at −80°C before mRNA analysis. For ex vivo MCF10.DCIS.com tumor slices, primary tumors were removed, cut by a scalpel and each tumor slide was placed over a metal grid inserted in a six-well plate to allow tumors to grow on an interface air/culture medium. Before imaging, 2.5 µg/ml doxycycline hyclate was added to the tumor slices culture media to induce RAB5A expression. Tumor cells were maintained under stimulation for five days, changing the medium every day. Tissue samples were fixed in 10% buffered formalin and embedded in paraffin. 4-µm tissue sections were counterstained with H&E and with indicated antibodies.

Neutral comet assay

Neutral comet assay was performed as already described[100] following the manufacturer's protocol (Trevigen). In summary, MCF10.DCIS.com cell monolayers were harvested by trypsinization, washed once in ice-cold PBS and resuspended in cold PBS at the final concentration of 1 x 10^5 cells/ml. Cell suspension was mixed with low-melting agarose at a ratio of 1:10 (v/v) and loaded onto comet slides. Samples were lysed in Lysis Solution over-night at 4 °C. Following electrophoresis in 1X Neutral Electrophoresis Buffer for 45 min at 21 V, slides were incubated in DNA Precipitation Buffer and washed once in 70% ethanol. Slides

were then dried up and DNA stained with SYBR Gold (Thermo-Fisher) prior to imaging. Comet tail moment was measured using OpenComet plug-in for ImageJ[101].

Laser-induced nuclear rupture and live-cell imaging

Cells were seeded on glass coverslips and cultured in complete medium until a uniform monolayer had formed. Cell culture medium has been refreshed before the live-imaging session.
Laser-induced nuclear rupture experiments were performed on an UltraVIEW VoX spinning-disk confocal system (PerkinElmer) equipped with an EclipseTi inverted microscope (Nikon) provided with a Nikon Perfect Focus System, an integrated FRAP PhotoKinesis unit (PerkinElmer) and a Hamamatsu CCD camera (C9100-50) and driven by Volocity software (Improvision; Perkin Elmer). All images were acquired through a 60X oil-immersion objective (Nikon Plan Apo VC, NA 1.4). After defining the region of interest, pre bleach images were collected for 30 seconds at a rate of 5 seconds per timepoint. Photobleaching was performed using UltraVIEW PK Device as a bleaching device on a small spot over the nuclear envelope. Images were captured for 300 seconds at a rate of 5 seconds per timepoint.

Image acquisition

Time-lapse imaging of the motility of 3D organoids was performed using a Leica TCS SP8 laser confocal scanner mounted on a Leica DMi8 microscope equipped with motorized stage; a HC PL FLUOTAR 20×/0.5 NA dry objective was used. A white-light laser was used as the illumination source. Leica Application Suite X (LAS X, https://www.leicamicrosystems.com/products/microscopesoftware/details/product/leica-las-x-ls/) was the software used for all the acquisitions. Image acquisition conditions were set to remove channel crosstalk, optimizing spectral detection bands and scanning modalities. ImageJ software was used for data analysis.
Operetta CLS, high-throughput spinning-disk confocal microscopy system (Perkin Elmer), by Harmony software 4.9. Cells are imaged with 20x water immersion objective NA 1.0
Confocal microscopy was performed with a Leica TCS SP5 confocal laser scanning system based on a Leica DMI 6000B inverted microscope. The images were acquired with a HCX PL APO 63X/1.4NA oil immersion objective. The software used for all acquisitions was Leica LAS AF. Laser lines: 405nm, 488nm, 561nm, 633nm.
Hypotonic-mediated cell streaming and EGFP-3NLS leakage time lapses were performed with a Leica Thunder Imaging System based on a Leica DMi8 inverted microscope equipped with a Leica DFC9000 GT sCMOS camera. The images were acquired with a HC PL APO 63X 1.4NA oil immersion objective (EGFP-3NLS time lapse) using Leica LAS X software.
Image acquisition of cGAS expression and localization on FFPE samples was performed with an Olympus BX63 full motorized wide field microscope equipped with a B/W Hamamatsu Orca_AG camera. the system is driven by Metamorph (Molecular Devices) software. We used UPlanApo 100x objective N.A.1.35

Growth assay Survival and broken nuclei discrimination

To evaluate the growth of MCF10.DCIS control empty vector mCherry H2B or RAB5A mCherry H2B a Harmony 4.9 (PerkinElmer) custom pipeline was implemented. After 3 days of treatment, the images were acquired. For each well (four wells each condition) composed by 89 fields, the pipeline identifies the nuclei on the gaussian filtered (radius 3 pixel) global image of mCherry channel using the B method of the Find Nuclei module (parameters were tuned condition by condition). Then the nuclei are filtered by intensity and morphological criteria. To discriminate broken and normal nuclei, the Linear Classifier module with 2 classes is used; the classifier was trained using around 30 nuclei both classes.

Image analyses

In order to count the number of Foci per Nuclei, a custom semi-automated Fiji[102, 103] plugin was developed. The plugin identifies on the Dapi/Nuclear Marker using Li (https://imagej.net/plugins/auto-threshold#li) Thresholding Schema on the filtered image (gaussian filter with radius 2 pixel). Nuclei are then splitting using watershed (https://imagej.net/plugins/classic-watershed)method and then checked and corrected by hand. For each nucleus, the plugin identifies and counts the foci on the Foci Channel Marker (53BP1 or γH2AX) using the ImageJ's Find Maxima (https://imagej.nih.gov/ij/docs/menus/process.html#find-maxima) plugin with the noise tolerance parameter selected by hand.
In order to count the number of Foci per Field Of View (FOV), a custom semi-automated Fiji[102, 103] plugin was developed. The plugin identifies on the Dapi/Nuclear Marker using Huang (https://imagej.net/plugins/auto-threshold#huang). Thresholding Schema on the filtered image (median

filter with radius 1 pixel). Nuclear structures were then split using watershed (https://imagej.net/plugins/classic-watershed) method and then checked and corrected by hand. For each FOV, the plugin identifies and counts micronuclear structures using ImageJ's Analyze Particles (https://imagej.net/imaging/particle-analysis) plugin with the size parameters selected by hand.

For assessing histone methylation on Lysine 27, fields of view were randomly selected based on nuclei signal, probed by DAPI staining. Images were analyzed using a custom semi-automated plugin developed in Fiji[102, 103]. Nuclei were identified on DAPI channel using StarDist plugin (https://imagej.net/plugins/stardist) with the built-in Versatile (fluorescent nuclei) neural network model. For each nuclear region of interest, the mean intensity was measured on the H3K27me3 channel and then normalized on the median of the mean intensity distribution of control cells.

For the analysis of the differential signal intensity at the nuclear periphery and central region, images were acquired and nuclei were segmented as described above. For each nuclear region of interest, the area was reduced to shrink it 1.5 µm from the nuclear border and the mean intensity in the H3K27me3 channel was calculated in the central nuclear region. Finally, the peripheral H3K27me3 mean intensity was calculated in the area comprised between the central region and the nuclear border.

Cell area fluctuation analysis

EGFP-E-cadherin expressing control and RAB5A-MCF10A cells were generated as described Cells were seeded in 6-well plate ($1.5*10^6$ cells/well) in complete medium and cultured until a uniform monolayer had formed. RAB5A expression was induced, were indicated, 16 hours before performing the experiment by adding fresh complete media supplemented with 2.5 µg/ml doxycycline to cells. Comparable cell confluence was tested by taking pictures by differential interference contrast (DIC) imaging using a 10x objective and counting the number of nuclei/field. To monitor cell fluctuations the phase contrast channel and EGFP-E-Cad channel were merged first and then the 2D videos were converted into 3D image stacks with x, y and t, as shown in the scheme (a). Based on the phase contrast image and the E-Cad signal, random selected cells are segmented and tracked semi-automatically using Segmentation Editor in Fiji (ImageJ plug-in). Cell boundaries were annotated manually with the interval of a few time points and then cell boundaries at other time points are interpolated in 3D to obtain accurate cell morphological dynamics along time. The segmentation and tracking results are shown in Fig. S2b. The random pseudo-color presents the cell identity for the visualization purpose. We can see that the cell tracking is represented as a "worm" structure in the space of x, y and t in 3D, while the RAB5 results are curlier than the Ctrl. The cell speed is calculated based the cell centroids and the cell area of each time points are also computed. As we have excellent temporal resolution, we assume that any deformation along the norm direction of a cell surface is small enough such that we can treat it as linear. Thus, we can estimate the deformation of a given cell along time. The negative and positive cell extension of the cell, as shown in Fig. 2F, can be quantitatively extracted. For a migrating cell, its surface can be described as a function of time, i.e. *S(x, y, t)*. The deformation between any two-time points is the partial differentiation of function S along t, given by:

$$\Delta S = \frac{\partial S}{\partial t} \qquad \text{Eq. (1)}$$

Based on our linear assumption, Eq. (1) is actually to find a linear minimum distance mapping for the points on the boundaries at two time points.

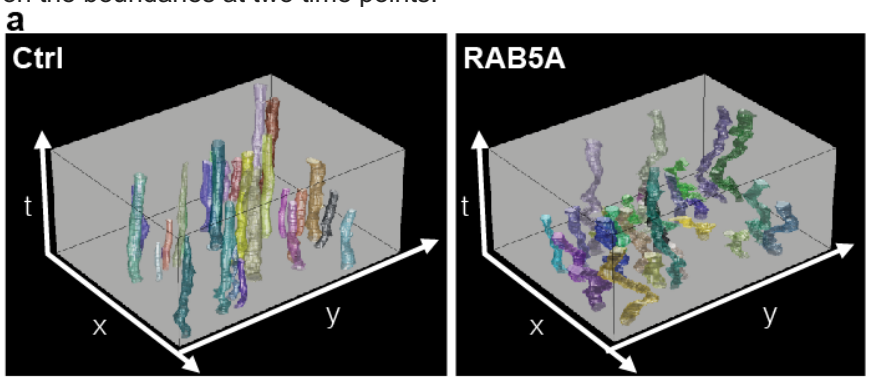

In the scheme (b), we demonstrate the cell boundaries of two consecutive points with the Maximum Positive Deformation (MPD) and Maximum Negative Deformation (MPD). The arrows show the marching points. We also need to define if the deformation is positive (extending) or negative (retracting). The positive

deformation means a boundary-points moving to a space which is not previously occupied by this cell, shown by the red arrows; while the negative deformation means a boundary point moving to a space which is previously occupied by this cell, shown as the blue arrow. To quantify the cell mobility, we defined the following 6 parameters:

1. Cell Area;
2. Cell Speed;
3. Maximum Deformation: The maximum norm of the positive deformation vectors, shown as the solid red arrow;
4. Minimum Deformation: The maximum norm of the negative deformation vectors, shown as the solid blue arrow.

Nuclei tracking and segmentation

Tracking and segmentation of single nuclei in sequencies of fluorescent microscopy images of confluent monolayers of mCherry-H2B cells is performed *via* a custom Matlab code implementing the following procedure.

Images are first corrected for background intensity inhomogeneities by applying the background removing algorithm described in detail in Ref.[104].

Random noise in each corrected image is then reduced by applying a Wiener filt[104]er, an adaptive noise-removal filtering that preserves nuclei edges while smoothing the white noise (see Eq. 9.44-9.46 in Ref.[105].

Nuclear segmentation obtained by applying a seeded watershed transform to each filtered image[106]. The "seeds" (i.e. the pixels that are set to zero in the image before applying the watershed transform) are determined as follows. A Laplacian-of-the-Gaussian (LoG) filter is applied to each filtered image, leading to a map L_G whose local minima correspond to the candidate centers of the nuclei. Differences in the fluorescent intensity of different nuclei are corrected by dividing L_G by an intensity map obtained *via* bicubic interpolation of the minima of L_G. The resulting map $\tilde{L}_G$ is binarized by setting to zero (one) all pixels whose value is above (below) a fixed threshold value k. Repeated pixel erosion operations are applied to the obtained binary mask to remove smallest features and separate partially overlapping nuclei, leading to a final binary map L_{BN} from which we extract the "seeds" to be used in the seeded watershed transform: internal "seeds" are obtained as the pixels where L_{BN} is non-zero, while external "seeds" as obtained the boundaries of the watershed transform of L_{BN}.

Once completed the segmentation procedure on a given image, we can determine the center of mass $\vec{x}_i$ of each nucleus in the image, its projected area A_i and the angle $\theta_{n,i}$ (modulo π) between the major axis of the nucleus and the x axis. The direction of the major axis is obtained as the direction of the eigenvector of the covariance matrix of the segmented area associated with the larger eigenvalue[107].

To reconstruct cell trajectories, we employ the Matlab code freely available at **http://site.physics.georgetown.edu/matlab/** implementing the algorithm developed by Crocker and Grier[108]. Once nuclei in different frames are linked into trajectories, the time evolution of the relevant single-nucleus parameters $\vec{x}_i(t)$, $A_i(t)$ and $\theta_{n,i}(t)$ can be determined.

The instantaneous velocity of the i-th nucleus at frame t is estimated as $\vec{v}_i(t) = \left(\vec{x}_{i+1}(t) - \vec{x}_{i-1}(t)\right)/2\delta t$, where δt is the time interval between two consecutive frames. The instantaneous mean migration velocity is computed as $\vec{v}_{cm}(t) = \langle \vec{v}_i(t) \rangle_i$, where $\langle \dots \rangle_i$ denotes the average over all the nuclei in the field of view (FOV). The amplitude of the velocity fluctuations is evaluated as the root mean square velocity of the nuclei in the center of mass reference frame $v_{rms}(t) = \sqrt{\langle |\vec{v}_i(t) - \vec{v}_{cm}(t)|^2 \rangle_i}$.

The velocity spatial correlation function is calculated as $C_{vv}(r) = \langle \langle \frac{\vec{v}_i(t)\cdot\vec{v}_j(t)}{|\vec{v}_i(t)|\cdot|\vec{v}_j(t)|} \delta(|\vec{x}_i(t) - \vec{x}_j(t)| - r) \rangle_{i,j} \rangle_t$ where i and j run over all the nuclei and t is averaged over the time window 4-20 h, unless otherwise indicated. An estimate of the correlation length L_c of the velocity field is obtained by fitting a stretched exponential model $e^{-\left(\frac{r}{L_c}\right)^{\alpha}}$ to $C_{vv}(r)$.

Visual inspection reveals that the described segmentation procedure is effective in identifying about 90-95% of the nuclei present in the field of view. Despite the effort to reduce multiple segmentation and nuclei merging, however, some segmentation errors occur, especially in those cases where the signal-to-noise ratio is low or partial superpositions of nuclei is frequent. To minimize the impact of segmentation errors on the analysis of nuclear features, we implemented a "quality filter" to remove potentially flowed measurements. To this end, we compute the total instantaneous intensity $J_i(t)$ integrating the image intensity $I(\vec{x}, t)$ over the segmented area of the i-th nucleus at frame t. We then compare the instantaneous

value $J_i(t)$ with its median $med[J_i(t')]_{i-11}^{i-1}$ evaluated over the previous 10 frames. If $\left|med[J(t')]_{i-11}^{i-1} - J_i(t)\right|/$ $med[J(t')]_{i-11}^{i-1}$ is larger than 0.1, the segmentation of the i-th nucleus at frame t is considered unreliable and the corresponding parameters are not included in the statistics. Trajectories which, after the application of the this "quality filter", lose more than 20% of frames because of this procedure are entirely excluded.

Particle image velocimetry

Particle image velocimetry (PIV) of fluorescent microscopy images of confluent monolayers of mCherry-H2B cells fluorescent images is performed by using the Matlab PIVLab software[109].

We choose an interrogation area with size slightly larger than the typical inter-nuclear distance, typically corresponding to 14 μm. Outliers in the reconstructed velocity field, whose modulus exceed a fixed threshold value, are identified and replaced with the median value of the velocity over neighboring grid points.

Nuclear deformation dynamics

In order to characterize nuclear shape fluctuations, we evaluate the mean square nuclear strain $MSS(\tau) = \langle\langle \Delta a_i{}^2(\tau|t) \rangle_t\rangle_i$ for different delay times τ. The nuclear strain $\Delta a_i(\tau|t)$ is estimated as $[A_i(t+\tau) - A_i(t)]/$ $\langle A_i(t)\rangle_t$, where $A_i(t)$ is projected area of the i-th nucleus at time t. To extract the key parameters characterizing nuclear deformation, we fit the model function $MSS(\tau) = \sigma_w + \dot{\gamma}_0\tau_c\left[1 - e^{-\tau/\tau_c}\right]$ to the data. This model, which includes a term σ_w accounting for the random noise in determination of the projected area, describes a diffusive-like growth of the area fluctuations with a characteristic strain rate $\dot{\gamma}_0$ for short delay times $MSS(\tau) \sim \dot{\gamma}_0\tau$, followed by a saturation to a plateau value $\dot{\gamma}_0\tau_c$ for long times. In figure 2G-H, the data and the best fitting curves are reported upon the subtraction of the baseline value σ_w obtained from the fitting procedure. Since the $MSS(\tau)$ does not always reach a clear plateau within the time window accessible during the experiments (Fig. 2G-H), there is a relatively large uncertainty in the determination of the overall amplitude $\dot{\gamma}_0\tau_c$ of the fluctuations. However, this does not affect the robustness of the estimate of $\dot{\gamma}_0$, as it characterizes the short time behavior of the fluctuations which is accurately sampled in our experiments.

Nuclei relative stiffness

In order to characterize the mechanical response of cell nuclei to intracellular stresses induced by mutual cell displacements, we evaluate independently nuclear and cell deformations by measuring the instantaneous nuclear strain rate and the corresponding instantaneous cell strain rate.

The first one is evaluated for a nucleus i at time t as $\dot{\gamma}_n(\vec{x}_i, t) = [a_i(t+\delta t) - a_i(t)]/\delta t$, where δt is the time interval between two consecutive acquired frames and $a_i(t) = A_i(t)/\langle A_i(t)\rangle_t$. From the instantaneous velocity field $\vec{v}(\vec{x}, t)$ obtained from PIV analysis we compute the divergence $div\ \vec{v}(\vec{x}, t) = \frac{\partial v_x(\vec{x},t)}{\partial x} + \frac{\partial v_y(\vec{x},t)}{\partial y}$. The divergence can be used as a proxy of the local deformation state of the monolayer. Qualitatively, a negative value of the divergence in a given position $\vec{x}$, indicates that cells are locally converging toward that point, leading to local compression (see Fig. 4A). *Vice versa*, positive values of divergence correspond to a local dilatation of the monolayer. In more rigorous terms, one can consider the local cell strain rate $\dot{\gamma}_c(\vec{x}, t) \equiv \frac{1}{A_c(\vec{x},t)}\frac{\partial A_c(\vec{x},t)}{\partial t}$, where $A_c(\vec{x}, t)$ is the cell area, *i.e.* the inverse of the local cell number density $\rho(\vec{x}, t)$. By using the continuity equation $div\ \vec{v}\rho = -\frac{\partial \rho}{\partial t}$, under the hypothesis of small density fluctuations, one gets $\dot{\gamma}_c(\vec{x}, t) \cong div\ \vec{v}(\vec{x}, t)$. This identity suggests that the mean square value of the divergence of the velocity field can be used to estimate the characteristic strain amplitude associated to monolayers internal deformations.

For every segmented nucleus i and time t , we consider the pair of values $[\dot{\gamma}_c(\vec{x}_i, t),\ \dot{\gamma}_n(\vec{x}_i, t)]$ obtained by associating the instantaneous nuclear strain rate $\dot{\gamma}_c(\vec{x}_i, t)$ with the corresponding cell strain rate $\dot{\gamma}_c(\vec{x}_i, t)$ in the position $\vec{x}_i(t)$, in the position $\vec{x}_i(t)$, estimated by bicubic interpolation of $div\ \vec{v}(\vec{x}, t)$. The data are shown in the scatter plot of Figure 4D-E after grouping into evenly spaced bins along the horizontal axis. In all investigated cases, we find a significant linear correlation between the two strain rates. Fitting a linear homogenous model to the data $\dot{\gamma}_n = s \cdot \dot{\gamma}_c$ enable estimating the dimensionless parameter s characterizing the relative deformation of a whole cell and the one of its nucleus. If we assume a minimalistic mechanical model, where the nucleus and the outer part of the cell are represented by two linear elements (whose deformation -or deformation rate- is proportional to the applied stress *via* a characteristic mechanical modulus) in series, our experimental findings enable interpreting the ratio $1/s$ between nuclear and whole cell strain rate as the ratio between the corresponding mechanical moduli or, in other terms, as the stiffness

of the nucleus normalized by the average stiffness of the whole cell. We note that, while the term "stiffness" may make think of an elastic-like response, we are not assuming here any specific model for the cell or the nuclear rheology. As a matter of fact, since the characteristic time scale of the considered fluctuations is very short and close to the inverse of the sampling frequency, in our experiments we are not able to accurately characterize the relative phase of nuclear and cellular deformation and thus to distinguish between a more liquid-like and a solid-like response.

Nuclear MSAD and velocity-orientation correlation

We measure the nuclear rotational dynamics through the analysis of the orientations $\theta_{n,i}(t)$ of the nuclei and of the direction of the instantaneous velocity $\theta_{v,i}(t)$, both obtained from PT.

The overall mean square angular displacement $MSAD(\tau)$ at a given time delay τ is evaluated averaging the single nuclei mean square angular displacements as $MSAD(\tau) = \langle \langle \Delta\theta_{n,i}{}^2(\tau|t) \rangle_t \rangle_i$ (Fig. S6D). We then fit the $MSAD$ with a ballistic-diffusive model $MSAD(\tau) = \sigma_{wr} + D_r \left[\tau + \frac{D_r}{\omega}\left(e^{-\tau\omega^2/D_r} - 1\right)\right]$, where D_r and ω are the rotational diffusion coefficient and the ballistic angular velocity, respectively. The term σ_{wr} is introduced to account for the random noise due to the segmentation errors. In Fig. S6D, the data and the best fit are reported upon the subtraction of the fitted σ_w.

In order to evaluate the degree of correlation between nuclear orientation and velocity we also considered the distribution of the angular difference $\Delta\theta_i(t) = \theta_{n,i}(t) - \theta_{v,i}(t)$, which is reported in Figure 6E as a polar plot. Absence of correlation corresponds to a uniform distribution of $\Delta\theta$. Conversely, the presence of a peak in the distribution for $\Delta\theta = 0$ indicates a tendency of the cell major axis of the nucleus to be oriented along the direction of cell velocity.

Immunostaining

As previously described[1], cells were washed twice with 1X PBS, fixed in 4% paraformaldehyde for 10 min and permeabilized with 0.1% Triton X-100 and 10% FBS for 10 min. After a 1X PBS wash, primary antibodies were added for 2 h at room temperature. Coverslips were washed in 1X PBS before secondary antibody incubation for 1 h at room temperature, protected from light. FITC-phalloidin was added in the secondary antibody step, where applicable. After removal of not specifically bound antibodies by 1X PBS washing, nuclei were stained with 0.5 ng ml–1 DAPI. Samples were post-fixed and mounted on glass slides in anti-fade mounting medium (glycerol). Antibodies were diluted in 1X PBS and 10% FBS.

Electron microscopy

Electron microscopic examination, immune EM gold labelling based on pre-embedding, EM tomography and correlative light-electron microscopy (CLEM) were performed as previously described[110-112]. A brief description of each process is presented below.

Embedding: Cells grown on MatTek glass bottom dishes (MatTek Corporation, USA) were fixed with 4% paraformaldehyde and 2,5% glutaraldehyde (EMS, USA) mixture in 0.1 M sodium cacodylate pH 7.4 for 2 h at RT, followed by 6 washes in 0.2 sodium cacodylate pH 7.2 at RT. Then cells were incubated in the 1:1 mixture of 2% osmium tetraoxide (OsO4) and 3% potassium ferrocyanide for 1 h at RT followed by 6 times rinsing in cacodylate buffer. Further, the samples were sequentially treated with 0.3% Thiocarbohydrazide in 0.2 M cacodylate buffer for 10 min and 1% OsO4 in 0.2 M cacodylate buffer (pH 6,9) for 30 min. Next, samples were rinsed with 0.1 M sodium cacodylate (pH 6.9) buffer until all traces of the yellow osmium fixative have been removed[16]. The samples were subsequently subjected to dehydratation in ethanol, embedded in Epoxy resin at RT, and polymerized for at least 72 h in a 60 °C oven.

ImmunoEM. Gold Enhancement: Cells grown on MatTeks were fixed with a mixture of 4% paraformaldehyde and 0.05% glutaraldehyde in 0.15M Hepes for 5 min at RT and then replaced with 4% paraformaldehyde in 0.15M Hepes for 30 min. Afterwards, the cells were washed 3 times in PBS and incubated with blocking solution for 30 min at RT. Then cells were incubated with primary anti GFP antibody (Abcam ab6556) a diluted 1:100 in blocking solution overnight at 4°C. On the following day, the cells were washed 3 times with PBS and incubated with goat anti-rabbit Fab' fragments coupled to 1.4nm gold particles (diluted in blocking solution 1:100) for 2h and washed 6 times with PBS. Meanwhile, the activated Gold Enhance TM-EM was prepared according to the manufacturer's instructions and 200 µl were added into each sample well. The reaction was monitored by a conventional light microscope and was stopped after 5-10 min when the cells had turned "dark enough" by washing several times with PBS. Then cells were fixed with of 2,5 % paraformaldehyde and 2,5% glutaraldehyde (EMS, USA) mixture in 0.1 M sodium cacodylate pH 7.4 for 2 h at RT, followed

by 6 washes in 0.1 sodium cacodylate pH 7.4 at RT. Then cells were incubated in 1:1 mixture of 2% osmium tetra oxide and 3% potassium ferrocyanide for 1 h at RT followed by 6 times rinsing in cacodylate buffer. Then the samples were sequentially treated with 0.3% Thiocarbohydrazide in 0.2 M cacodylate buffer for 10 min and 1% OsO4 in 0.2 M cacodylate buffer (pH 6,9) for 30 min. The samples were subsequently subjected to dehydratation in ethanol, and embedded in Epoxy resin at RT and polymerized for at least 72 h in a 60 °C oven[111].

Sectioning: The cell of interest was selected during the analysis of the MatTek and then this cell was subjected to the optical sectioning and the Z-stacking was performed using confocal microscope. Then, the sample was subjected to the procedure of immune EM labelling with an antibody against the defined proteins (antigens) using the Nanogold enhancement procedure as it was described[111, 112]. Z-stack images were printed and during trimming of the pyramid and its sharpening these images were constantly used for orientation. Embedded samples were then sectioned with diamond knife (Diatome, Switzerland) using Leica EM UC7 ultra microtome. Sections were analyzed with a Tecnai 20 High Voltage EM (FEI, Thermo Fisher Scientific; The Netherlands) operating at 200 kV.

EM Tomography: Two-step CLEM based on the analysis of tomographic reconstructions acquired under low magnification with consecutive reacquisition of EM tomo box under high magnification and its re-examination was used exactly as described[111]. Briefly, an ultramicrotome (Leica EM UC7; Leica Microsystems, Vienna) was used to cut 200 nm serial semi-thick sections. Sections were collected onto 1 % Formvar films adhered to slot grids. Both sides of the grids were labelled with fiduciary 10 nm gold (PAG10, CMC, Utrecht, the Netherlands). Tilt-series were collected from the samples from ± 65° with 1° increments at 200 kV in Tecnai 20 electron microscopes (FEI, Thermo Fisher Scientific, Eindhoven, the Netherlands). Tilt series were recorded at a magnification of 9,600x, using software supplied with the instrument. The nominal resolution in our tomograms was 4 nm, based upon section thickness, the number of tilts, tilt increments, and tilt angle range. The IMOD package and its newest viewer, 3DMOD 4.0.11, were used to construct individual tomograms and for the assignment of the outer leaflet of organelle membrane contours, CLEM was performed exactly as described[110].

Statistical analysis

All data are presented as scatter plots or box plots expressed as mean ± standard deviation (s.d.) unless otherwise indicated. The number of experiments as well as the number of samples analyzed is specified for each experiment and reported in the figure legends. Statistical significance was calculated, whenever we compared two distinct distributions, using a parametric two-tails unpaired student's t-test with Welch corrections for two samples with un-equal variance or non-parametric two-tails Mann-Whitney t-test as indicated. Nested one-way ANOVA was used as reported for comparison of more unmatched groups. Significance was defined as $*p < 0.05$; $**p < 0.01$; $***p < 0.001$ and $****p < 0.0001$. Statistical calculations were performed with GraphPad Prism 8 Software or Microsoft Excel software.

Figure S1

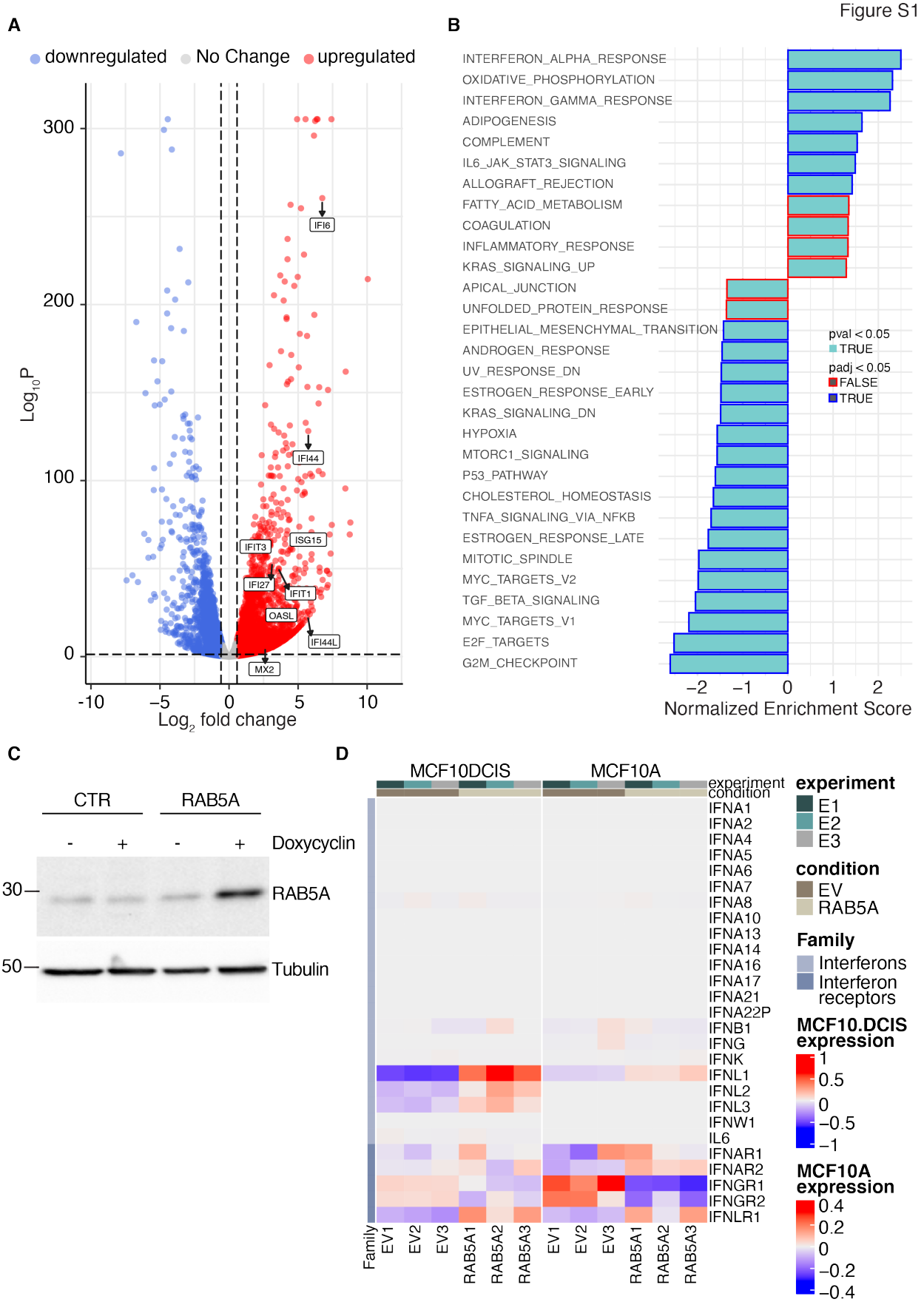

1583

Figure S1. Tissue fluidification induces a CytoDR gene signature in MCF10 monolayers and has marginal effect on Interferon and Interferon receptor genes

A. Volcano plot representing differentially expressed genes between control empty vector and RAB5A-expressing MCF10A monolayers. All significantly RAB5A-expressing deregulated genes are indicated in red (upregulated) and blue (downregulated). The enrichment (log2Fold Change) is plotted on the x-axis and the significance (Wald test -log10 p value) is plotted on the y-axis. Labels show genes validated in Fig. 1D.

B. Gene set enrichment analysis (GSEA) of differentially expressed genes in RAB5A-expressing MCF10A monolayer over control cells. GSEA was performed using the Hallmarks pathway gene sets in the GSEA Molecular Signatures Database. Moderated t-statistic was used to rank the genes. Reported are significantly enriched pathways (P-value < 0.05) with the color of the outline of the bar corresponding to the BH-adjusted P-value. P-value was calculated as the number of random genes with the same or more extreme ES value divided by the total number of generated gene sets.

C. Immunoblots of lysates from doxycycline-treated control (CTR) and RAB5A-expressing (RAB5A) MCF10.DCIS.com monolayers with the indicated antibodies. Mw are indicated on the left.

D. Heatmap showing the relative expression of interferon and interferon receptor genes in each of the 3 replicates of the conditions control empty vector (EV) and RAB5A-expressing (RAB5A) respectively in MCF10.DCIS and MCF10A monolayers.

Figure S2

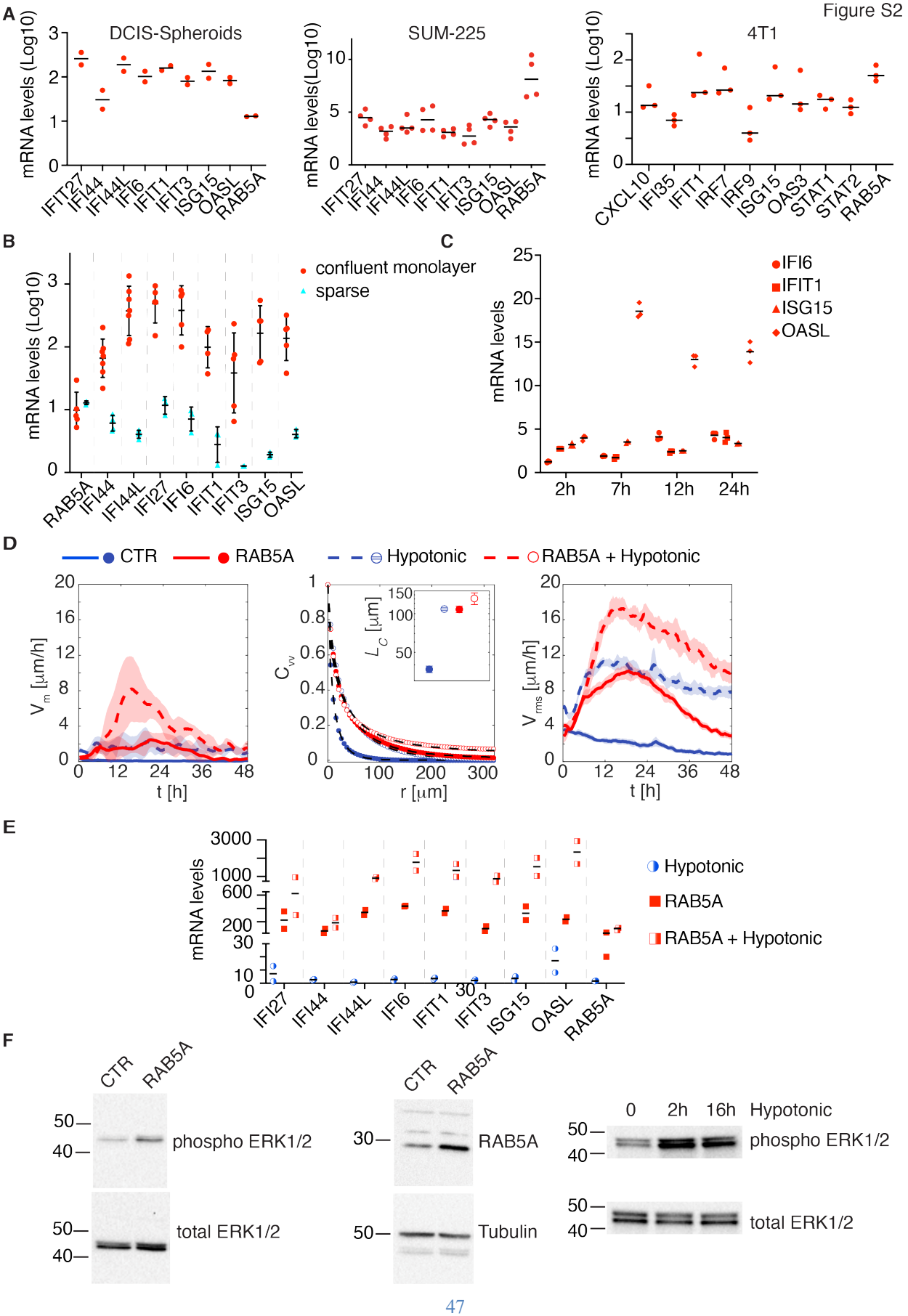

1604

Figure S2. Tissues fluidification induces CytoDR gene expression in various normal and tumoral epithelia

A. Scatter plots of the mRNA expression levels of IFI27, IFI44, IFI44L, IFI6, IFIT1, IFIT3, ISG15, OASL and RAB5A determined by qRT-PCR in different RAB5A-expressing cell lines over the respective control cells (3D MCF10.DCIS.com spheroids, SUM-225 and 4T1monolayers). Data are the mean (at least n = 2 independent experiments). Values were normalized to the controls in each experiment.

B. Scatter plots of the mRNA expression levels of RAB5A, IFI44, IFI44L, IFI27, IFI6, IFIT1, IFIT3, ISG15 and OASL determined by qRT-PCR in doxycycline-treated RAB5A-expressing MCF10.DCIS.com monolayers or sparsely seeded cells (sparse) over the corresponding control cells. Data are the mean ± s.d. (n=3 independent experiments). Values were normalized to the controls of each experiment.

C. Scatter plots mRNA expression levels of IFI6, IFIT1, ISG15 and OASL determined by qRT-PCR in MCF10.DCIS.com cells incubated with hypotonic medium at the indicated time points. Data are expressed as mean (n = 3 independent experiments). Values were normalized to the controls of each experiment.

D. Migration parameters of control (CTR) or RAB5A-expressing (RAB5A) MCF10.DCIS.com monolayers treated with hypotonic media for 48 h (see Movie S1), obtained from PIV analysis. Left panel: migration speed v_m. Central panel: spatial velocity correlation functions C_{vv} evaluated over the time window 8-40 h. In the inset are reported the corresponding correlation lengths L_c obtained from stretched exponential fits on C_{vv} curves (black dashed lines in the main panel). Right panel**:** root mean square velocities in the center of mass reference frame. Velocity fields are computed over 4 FOVs per condition (each FOV including more than 2 10^3 cells). The width of each of the shaded regions reported in the left and in the right panel corresponds to 2 times the standard deviation of the corresponding variable, evaluated over different FOVs.

E. Scatter plots of the mRNA expression levels of IFI27, IFI44, IFI44L, IFI6, IFIT1, IFIT3, ISG15, OASL and RAB5A determined by qRT-PCR in MCF10.DCIS.com monolayers subjected to different conditions (doxycycline-induction of RAB5A-expression, hypotonic treatment or the combination of both) over control cells. Data are the mean (n = 2 independent experiments). Values were normalized to the controls of each experiment.

F. Immunoblots with the indicated antibodies from doxycycline-treated lysate of control (CTR) and RAB5A-expressing (RAB5A) monolayers or from hypotonic treated cells at the indicated time points. Mw are indicated on the left.

1636

Figure S3

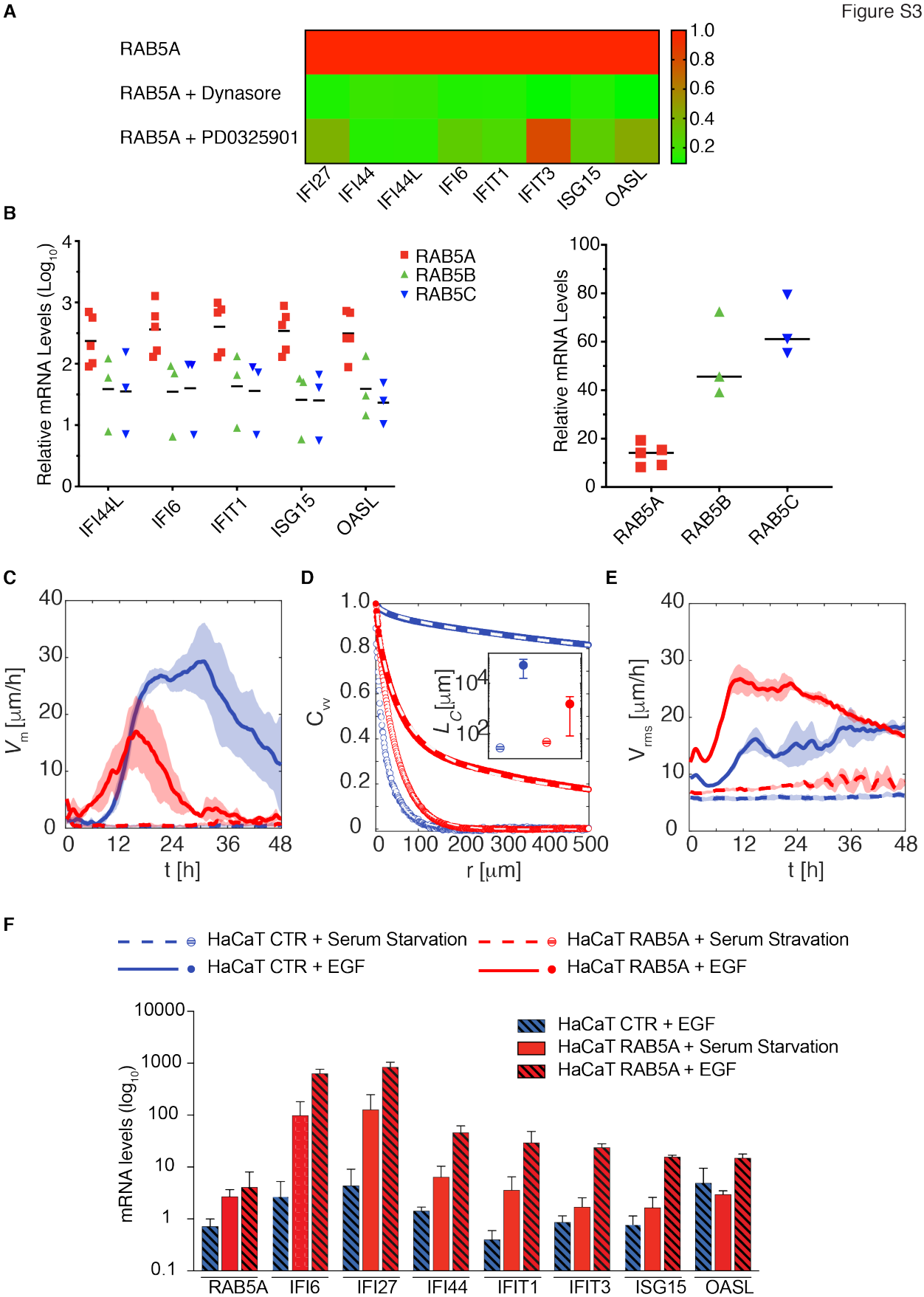

1637

Figure S3. Tissue fluidification-dependent CytoDR is mediated by RAB5A in MCF10.DCIS.com and HaCat.

A. Heatmap representing color-coded expression levels of differentially expressed CytoDR genes in RAB5A-expressing MCF10.DCIS.com monolayer treated as indicated. The data are the ratio of relative level of gene expression compared to RAB5A-expressing cells expressed as mean ± s.d. (at least n = 3 independent experiments). P values, each-pair Student's t-test (treated versus RAB5A-expressing cells) are reported in Table Figure S3A.

B. Scatter plot of the mRNA expression levels of IFI44L, IFI6, IFIT1, ISG15 and OASL (left panel) determined by qRT-PCR in MCF10.DCIS.com monolayer expressing RAB5A, RAB5B or RAB5C (right panel) over control cells. Data are expressed as mean (at least n = 3 independent experiments). Values were normalized to the controls of each experiment.

C-E. Migration parameters of HaCat monolayers, obtained from nuclear tracking. Doxycycline-treated control or RAB5-expressing HaCat monolayers were serum starved (SS) for 48 h before addition of 100 ng/ml of EGF and monitored by time lapse microscopy (see Movie S2). (**C**) Migration speed v_m. (**D**) Spatial velocity correlation functions C_{vv} evaluated over the time window 8-40 h. In the inset we report the corresponding correlation lengths L_c obtained from stretched exponential fits on C_{vv} curves (black dashed lines in the mail panel). (**E**) Root mean square velocities in the center of mass reference frame. Velocity fields are computed over different FOVs, encompassing in total about 10^4 tracked cells per frame per condition. The width of each of the shaded regions reported in the left and in the right panel corresponds to 2 times the standard deviation of the corresponding variable, evaluated over different FOVs.

F. Box plot of the mRNA expression levels of RAB5A, IFI6, IFI27, IFI44, IFIT1, IFIT3, ISG15 and OASL determined by qRT-PCR in doxycycline-treated control (CTR) and RAB5A-expressing HaCat monolayers treated exactly as described above with respect to control cells. Monolayers were serum starved mock treated or stimulated with 100 ng/ml EGF: Hatched blue bar, serum starved HaCat CTR + EGF; Red bars, HaCat RAB5A- serum starved; hatched red bar, serum starved HaCat RAB5A stimulated with 100 ng/ml EGF (Serum Starved HaCat RAB5A = EGF) over control serum starved HaCat cells. Data are expressed as mean ± s.d. (at least n = 3 independent experiments). Values were normalized to the controls of each experiment.

Figure S4

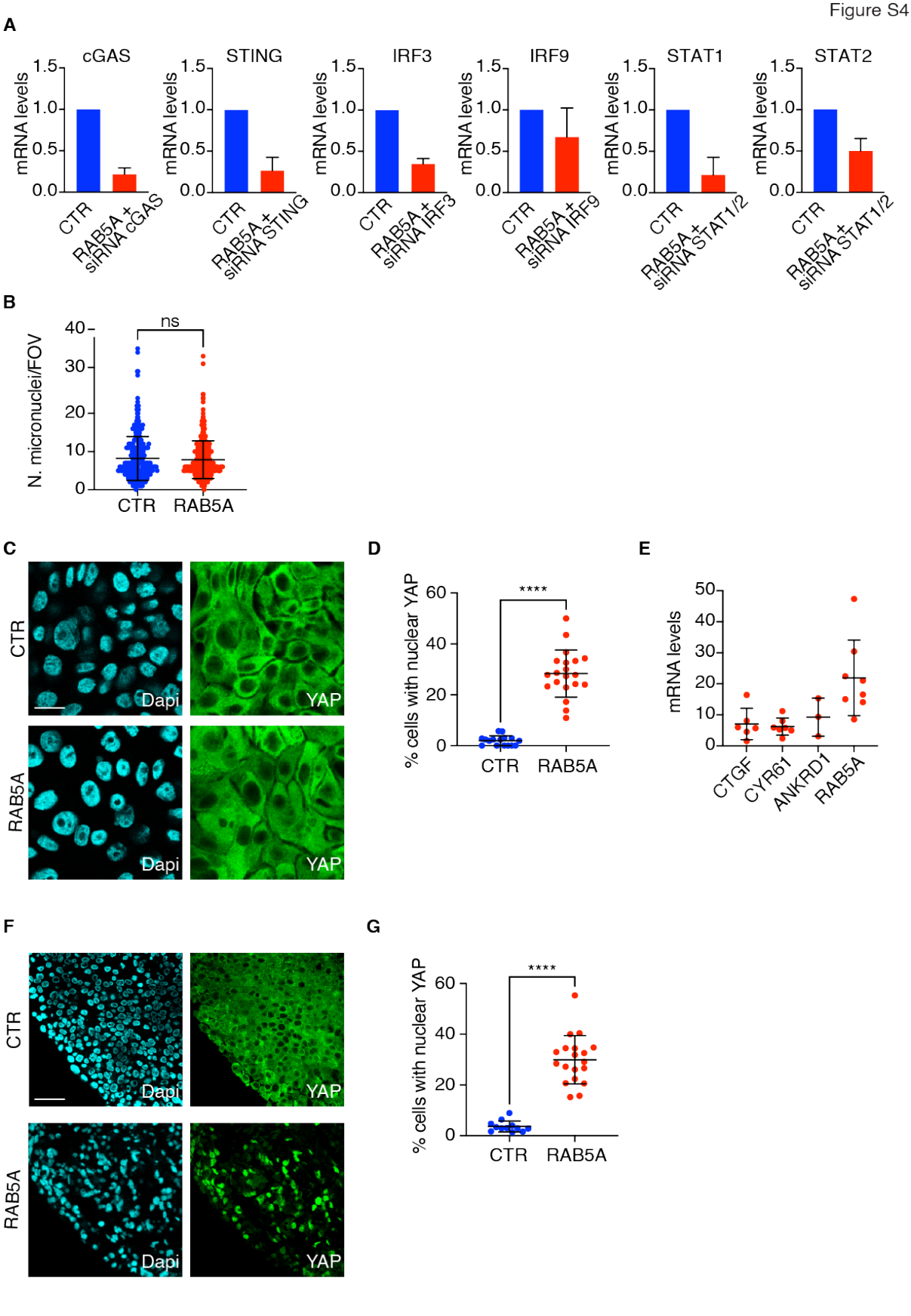
A
cGAS
STING
IRF3
IRF9
STAT1
STAT2
mRNA levels
1.5
1.0
0.5
0.0
CTR
RAB5A + siRNA cGAS
RAB5A + siRNA STING
RAB5A + siRNA IRF3
RAB5A + siRNA IRF9
RAB5A + siRNA STAT1/2
B
N. micronuclei/FOV
40
30
20
10
0
ns
CTR
RAB5A
C
CTR
RAB5A
Dapi
YAP
D
% cells with nuclear YAP
60
40
20
0
****
CTR
RAB5A
E
mRNA levels
50
40
30
20
10
0
CTGF
CYR61
ANKRD1
RAB5A
F
CTR
RAB5A
Dapi
YAP
G
% cells with nuclear YAP
60
40
20
0
****
CTR
RAB5A

Figure S4. Tissue fluidification activates the mechano-transducer YAP1

A. Box plot of the mRNA expression levels of cGAS, STING, IRF3, IRF9, STAT1 and STAT2 determined by qRT-PCR in RAB5A-expressing MCF10.DCIS.com monolayer over control cells silenced with indicated oligos. Data are expressed as mean ± s.d. (at least n = 3 independent experiments). Values were normalized to the controls of each experiment.

B. Number of micronuclei per field of view (FOV) in control (CTR) and RAB5A-expressing MCF10.DCIS.com monolayers is expressed as the mean ± s.d. (at least $n = 100$ FOV/experimental conditions in three independent experiments). ns>0.999, P values, each-pair Mann Whitney test (CTR versus RAB5A).

C. Immunofluorescence images of control (CTR) and RAB5A-expressing (RAB5A) MCF10.DCIS.com monolayers stained with Dapi and anti-YAP antibody to detect nuclei and YAP localization, respectively. Scale bar 40 μm.

D. Scatter plot of the percentage of cells with nuclear YAP is expressed as the mean ± s.d. (at least $n = 5$ FOV/experimental conditions in three independent experiments). ****$p < 0.0001$, P values, each-pair Welch's test (CTR versus RAB5A).

E. Scatter plot of the mRNA expression levels of CTGF, CYR61, ANKRD1 and RAB5A determined by qRT-PCR in RAB5A-expressing MCF10.DCIS.com monolayers over control cells. Data are from at least 3 independent experiments. Values were normalized to the controls of each experiment.

F. Immunofluorescence images of control (CTR) and RAB5A-expressing (RAB5A) MCF10.DCIS.com injected into mammary fat pads of immunocompromised mice. After four weeks, primary tumors were isolated, sectioned and cultivated as organotypic tumor slices for 6 days at air-liquid interface over a synthetic membrane. After adding doxycycline to induce RAB5A expression, the slices were fixed and stained with Dapi and YAP to detect nuclei and YAP localization, respectively. Scale bar 100 μm.

G. Scatter plot of the percentage of cells with nuclear YAP is expressed as the mean ± s.d. (at least $n = 4$ FOV/experimental conditions in three independent experiments). ****$p < 0.0001$, P values, each-pair Welch's test (CTR versus RAB5A).

Figure S5

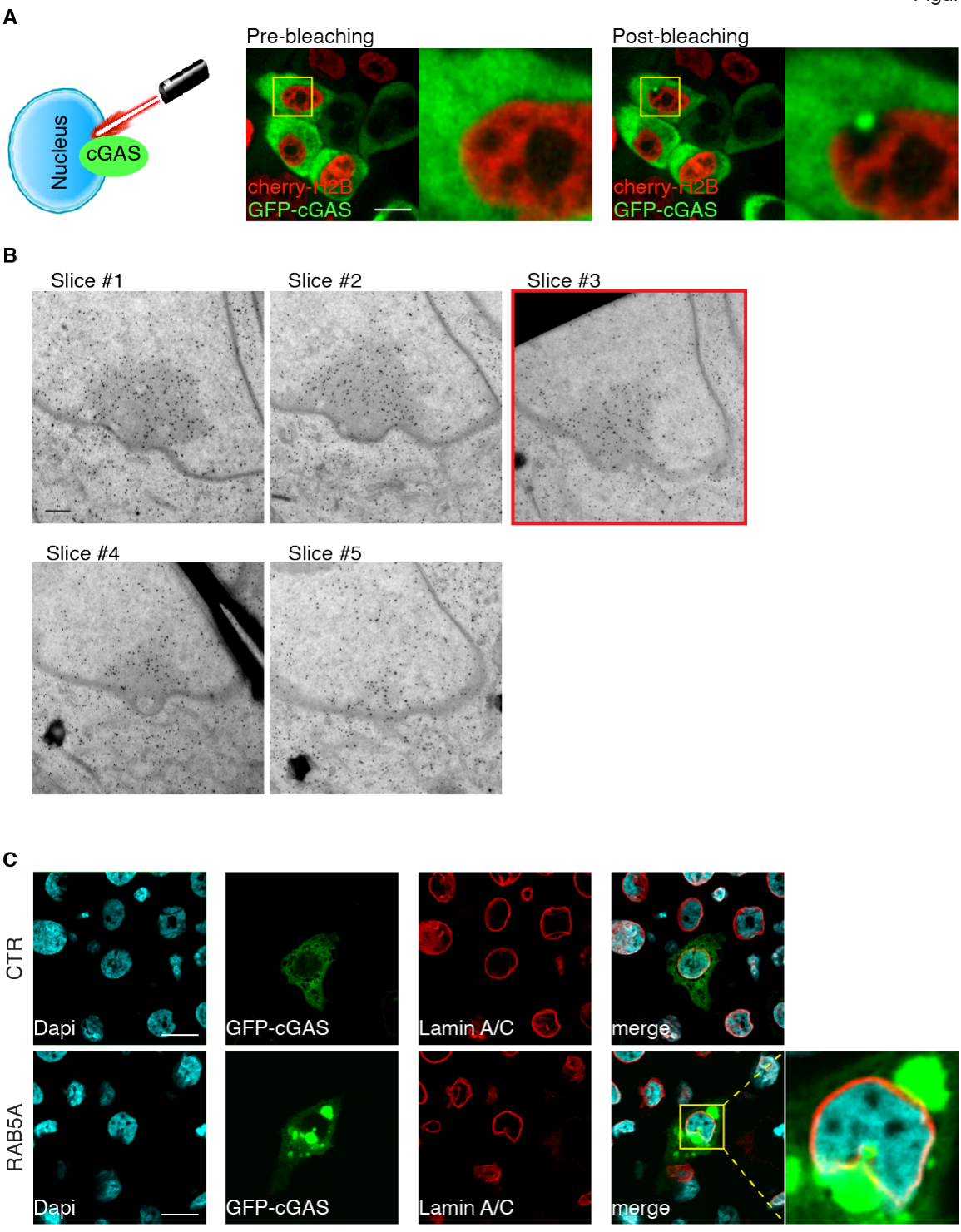

Figure S5. cGAS accumulation at nuclear envelope ruptures

A. Schematic overview of experimental procedures for NE laser ablation (left panel). Snapshot of stable EGFP-cGAS/mcherry-H2B MCF10.DCIS.com monolayers (right panel). Magnified images from the selected boxed area are shown. Scale bar 20 μm.

B. Sequential Z axis sections of EGFP-cGAS-expressing RAB5A-MCF10.DCIS.com monolayers used for 3D tomographic reconstruction shown in Figure 3F (lower right image). The image outlined in red correspond the one shown in Figure 3F (upper right image). Scale Bar, 500 nm.

C. Immunofluorescence images of control (CTR) and RAB5A-expressing (RAB5A) MCF10.DCIS.com monolayers transiently transfected with EGFP-cGAS and stained with Dapi and anti-Lamin A/C antibody to detect nuclei and nuclear lamina, respectively. Magnified images of the selected boxed area are shown. Scale bar 20 μm.

Figure S6

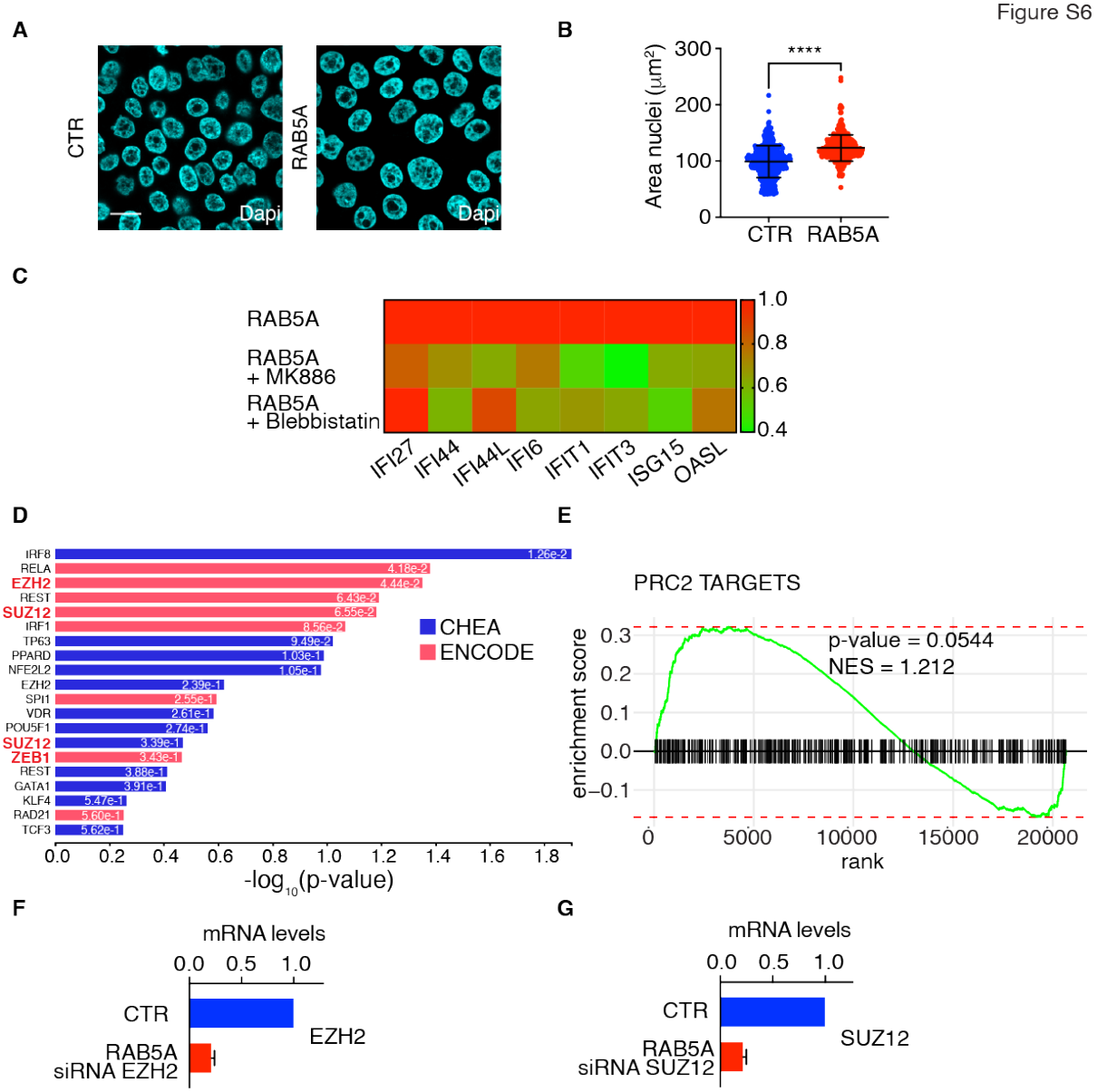

Figure S6. Fluidized MCF10.DCIS.com monolayers display an increase nuclear size and enrichment in PRC2-targets

A. Immunofluorescence images of control (CTR) and RAB5A-expressing (RAB5A) MCF10.DCIS.com monolayers stained with Dapi to detect nuclei. Scale bar 20 μm.

B. Scatter Plot of the nuclear area per field of view is expressed as the mean ± s.d. (at least $n = 100$ FOV/experimental conditions in three independent experiments). ****$p < 0.0001$, P values, each-pair Mann Whitney test (CTR versus RAB5A).

C. Heatmap representing color-coded expression levels of differentially expressed CytoDR genes in RAB5A-expressing MCF10.DCIS.com monolayers treated with vehicle or with MK-886 that inhibits 5-lipoxygenase-activating protein (FLAP) and COX-1[113] or Blebbistatin. The data are the ratio between the level of gene expression in each of the conditions tested relative to those of vehicle-treated RAB5A-expressing cells expressed. The mean ± s.d. (at least n = 3 independent experiments) and P values, each-pair Student's t-test (treated versus RAB5A-expressing cells) are reported in Table Figure S6E.

D. Transcription factor enrichment analysis for overlap between the input set of differentially expressed genes in MCF10.DCIS.com monolayer over control cells and entries of the ChEA and ENCODE databases. Reported in the bars is the P-value (combination of Fisher's exact test and deviation from expected rank

for random input gene-set). Bars are colored according to the transcription factor/target-gene interactions from ChIP-seq/chip experiments database where they have been found enriched.
E. GSEA Enrichment plot of the PRC2 targets gene set in the CGP collection of the GSEA Molecular Signatures Database using differentially expressed genes in RAB5A-expressing MCF10.DCIS.com monolayer. The green curve corresponds to the ES (enrichment score) curve, which is the running sum of the weighted enrichment score obtained from GSEA software, while the normalized enrichment score (NES) and the corresponding P-value are reported within the graph.
F-G. Box plot of the mRNA expression levels of EZH2 and SUZ12 determined by qRT-PCR in RAB5A-expressing MCF10.DCIS.com monolayer over control cells silenced with the indicated oligos. Data are the mean ± s.d. (n = 3 independent experiments). Values were normalized to the controls of each experiment.

Figure S7

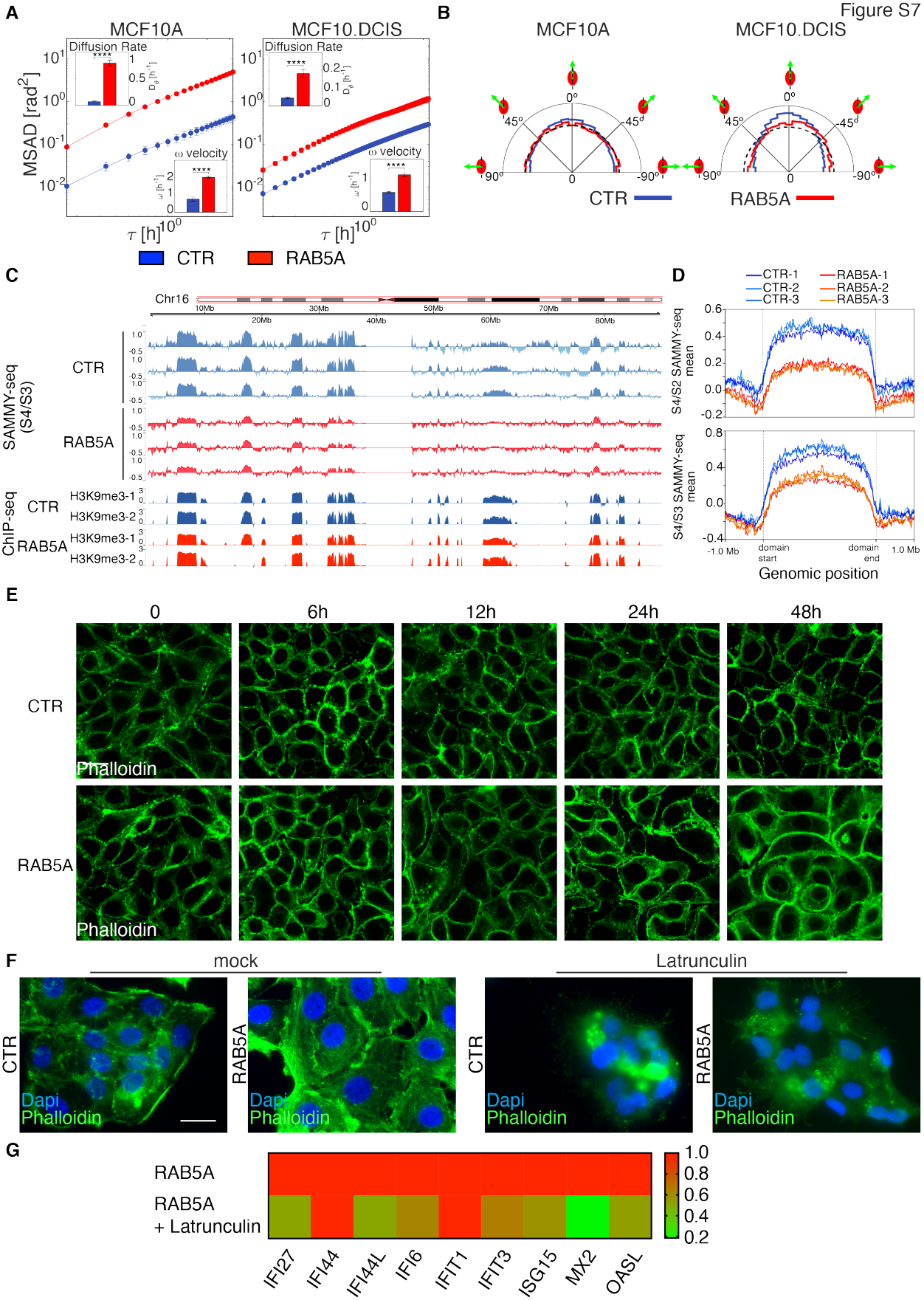

1743

Figure S7. Tissues fluidification promotes nuclear rotation, H3K9me3 reorganization and perinuclear actin remodeling

A. Nuclear mean square angular displacement (MSAD) in MCF10A and MCF10.DCIS.com monolayer, comparing control and RAB5A-expressing cells. In each condition, the MSAD is obtained by tracking and segmenting n nuclei over the time window 4-20 h (n>5000 and n>1000 for control and RAB5A-expressing MCF10A monolayers, respectively; n>700 and n>400 for control and RAB5A-expressing MCF10.DCIS.com monolayers, respectively). Insets: corresponding diffusion rate D_θ and angular velocity ω obtained by fitting the MSAD curves with a model function (continuous lines in the main panels) describing the transition from a short-time ballistic to a long-time diffusive behavior. Results are the mean ± s.d. (n= randomly populated subsets of cells). ****p < 0.0001, P values, T test (CTR versus RAB5A).

B. Polar histograms representing the probability distribution functions (PDFs) of the angle between cell velocity (estimated from nuclear tracking) and direction of the major axis of its nucleus. Dashed black lines represent the uniform distribution, corresponding to a complete absence of correlation between cell velocity and nuclear orientation.

C. Visual representation of genomic tracks for ChIP-seq signal enrichment and SAMMY-seq fractions comparison for a representative chromosome (chr 16). For each position along the chromosome (x axis) the enrichment signal (y axis) is reported as the normalized log2 ratio of ChIP over input control samples sequencing reads for ChIP-seq and the normalized log2 ratio of S4 over S3 sequencing (S4/S3) for SAMMY-seq. The data shown in the genomic tracks (from top to bottom) are: three SAMMY-seq replicates on CTR and RAB5A samples; two H3K9me3 ChIP-seq replicates (performed with two alternative antibodies - see methods) on CTR and RAB5A.

D. Average SAMMY-seq enrichment signal over heterochromatic regions (metaprofile). SAMMY-seq experiment profiles computed on CTR and on RAB5A over-expression samples are reported (three replicates for each condition depicted with lines of different colors - see color legend). The heterochromatic regions were selected based on H3K9me3 ChIP-seq (with ab-176916-Abcam antibody) enriched domains (n=78 domains). The x-axis reports the relative position with respect to the start and end borders of the considered domains (domain bodies rescaled) in addition to 1Mb flanking regions with absolute (unscaled) coordinates. The y-axis reports the average SAMMY-seq enrichment across all the considered domains. Similar results are obtained by considering either the S4/S2 or the S4/S3 SAMMY-seq fractions comparisons (log2 ratios) to highlight the location of the less accessible and soluble chromatin fraction.

E. Immunofluorescence images of a time course analysis in control (CTR) and RAB5A-expressing (RAB5A) MCF10.DCIS.com monolayers stimulated with doxycycline to induce RAB5A expression, fixed at indicated time points and stained with phalloidin to detect F-actin. Scale bar 30 μm.

F. Images of control (CTR) and RAB5A-expressing (RAB5A) MCF10.DCIS.com monolayers treated with w/o Latrunculin and stained with the Dapi and Phalloidin to detect nuclei and F-actin respectively. Scale bar, 20 μm.

G. Heatmap representing color-coded expression levels of differentially expressed CytoDR genes in RAB5A-expressing MCF10.DCIS.com monolayer treated as indicated. The data are the ratio between the level of gene expression in each of the conditions tested relative to those of mock-treated RAB5A-expressing cells. The mean ± s.d. (at least n = 3 independent experiments) and P values, each-pair Student's t-test (treated versus RAB5A-expressing cells) are reported in Table Figure S7E.

Figure S8

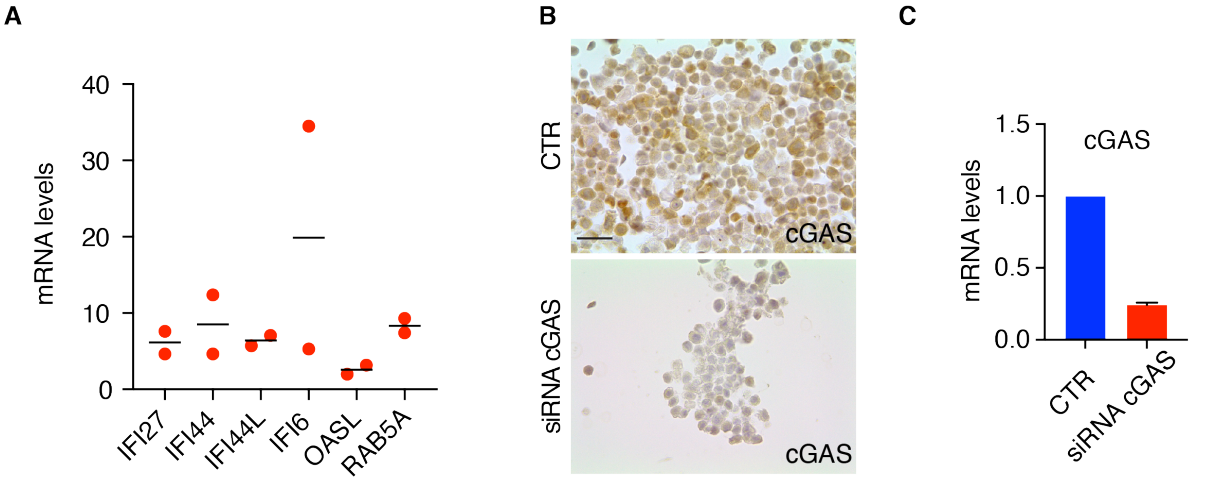

Figure S8. CytoDR genes are induced in RAB5A-expressing MCF10.DCIS.com tumor xenograft and validation of anti-cGAS antibody

A. Scatter plot of the mRNA expression levels of IFI27, IFI44, IFI44L, IFI6, OASL and RAB5A determined by qRT-PCR in RAB5A-expressing MCF10.DCIS.com over control cells injected into mammary fat pads of immunocompromised mice. After one week, mice were fed with doxycycline to induce RAB5A expression and the primary tumors were isolated four weeks after doxycycline treatment, lysed and processed for total RNA extraction. Data are the mean (n = 2 independent experiments). Values were normalized to the controls of each experiment.

B. IHC validation of the of cGAS antibodies using control (CTR) and cGAS silenced MCF10.DCIS.com cells. After silencing, cells were pelleted, included in agarose gel and fixed. Samples were embedded in paraffin, processed and stained with cGAS antibody.

C. Box plot of the mRNA levels of cGAS determined by qRT-PCR in MCF10.DCIS.com monolayer over control cells silenced with the indicated oligo. Data are expressed as mean ± s.d. (n = 3 independent experiments). Values were normalized to the controls of each experiment.

Figure S9

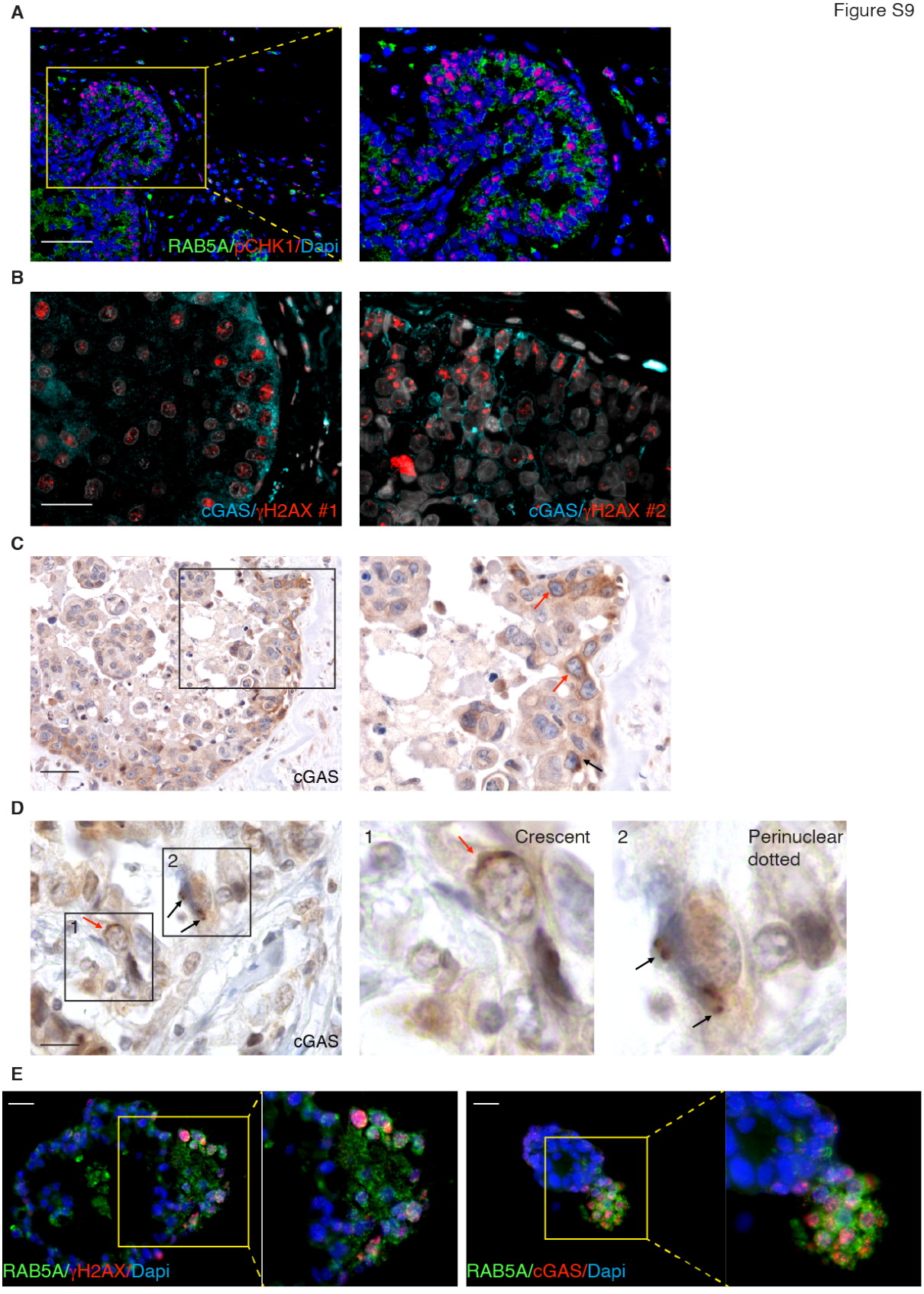
A
RAB5A/pCHK1/Dapi
B
cGAS/γH2AX #1
cGAS/γH2AX #2
C
cGAS
D
1
2
cGAS
1
Crescent
2
Perinuclear
dotted
E
RAB5A/γH2AX/Dapi
RAB5A/cGAS/Dapi

Figure S9. IHC characterization of RAB5A, pChk1 and cGAS in human DCIS and breast cancer organoids

A. Representative (1 out of more than 20 tested) multiplex immunohistochemistry/immunofluorescence (mIHC/IF) of RAB5A, pCHK1 and Dapi in human Ductal breast Carcinoma *in Situ* (DCIS). A magnified image from the selected yellow boxes is shown. Scale bar 250 μm.

B. Representative multiplex OPAL immunohistochemistry/immunofluorescence (mIHC/IF) of cGAS and γH2AX in two distinct human DCIS. Scale bar 100 μm.

C. Representative immunohistochemistry analysis of cGAS in human DCIS with invasive buds. A magnified image from the selected boxed area is shown. Red Arrow indicate the crescent-like, perinuclear accumulation of cGAS signal. Scale bar 80 μm.

D. Representative immunohistochemistry analysis of cGAS in locally invasive human DCIS. Magnified images from the selected boxed area are shown. Red arrow indicates the crescent-like, perinuclear accumulation of cGAS signal, black arrows indicate the perinuclear dotted distribution of cGAS. Scale bar 40 μm.

E. Representative multiplex immunohistochemistry/Immunofluorescence (mIHC/IF) of RAB5A, γH2AX, cGAS and Dapi in patient-derived breast cancer organoids. Magnified images from the selected yellow boxes are shown. Scale bar 150 μm.

Figure S10

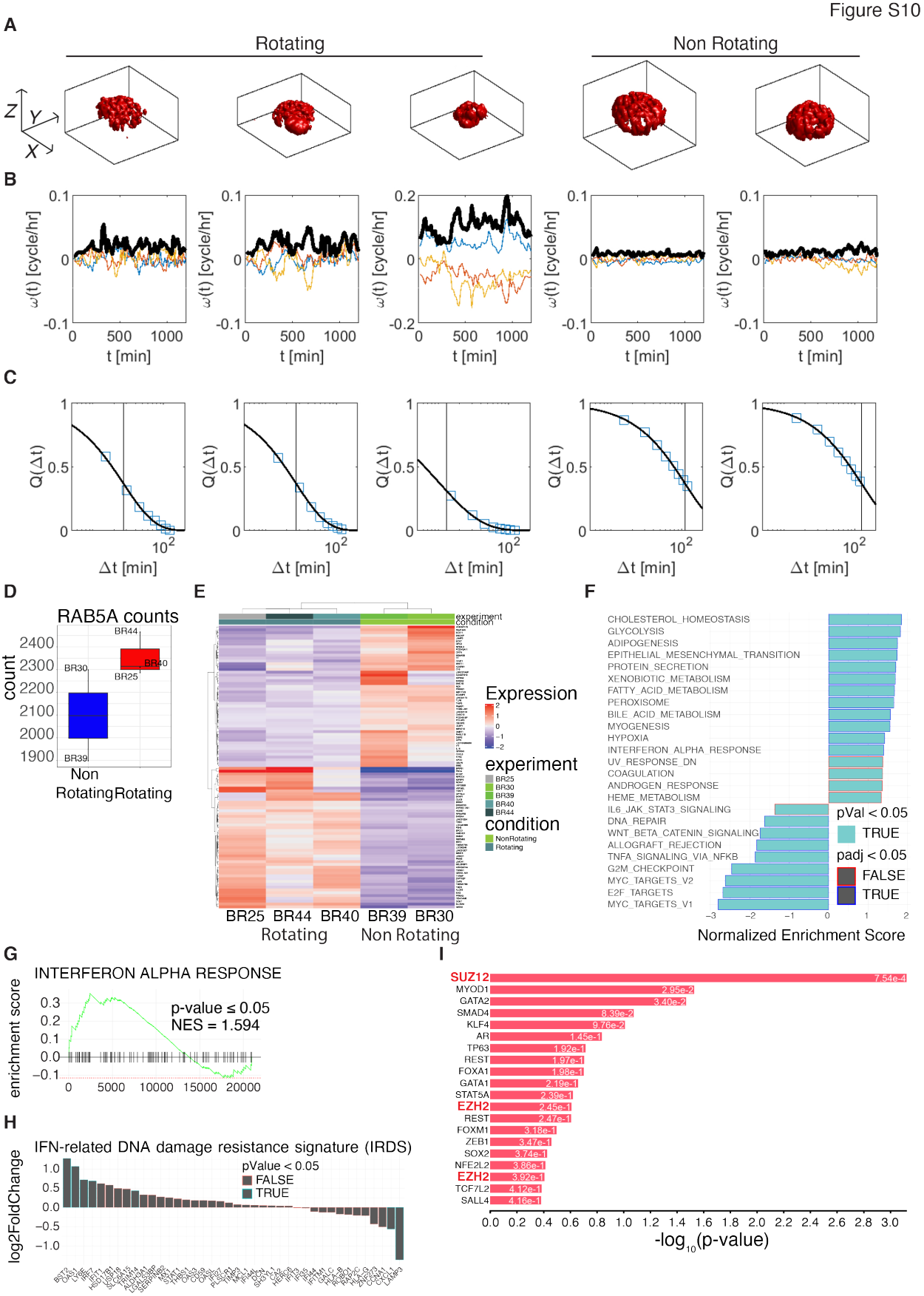

1827

Figure S10. Human breast cancer organoids that persistently rotate display elevated RAB5A, and enrichment in ISG and PRC2-dependent genes

A. 3D rendering of 5 living breast cancer organoids. The size of each box along the x- and y-directions corresponds to 200 μm.

B. Thin blue, orange and yellow curves: temporal evolution of the x, y and z components of the angular velocity associated with the rotation of the organoid depicted in the box above each panel, respectively. Thick black curves represent the angular speed, *i.e.,* the modulus of the angular velocity. Organoids are categorized as "rotating" if their average angular speed is larger than $0.03\,\mathrm{cycles/h}$, as "non rotating" otherwise.

C. Symbols: overlap parameter $Q(\tau)$ obtained from 3D-DVA analysis, capturing the internal rearrangement dynamics of the organoid depicted in the box above each panel. Continuous thin lines are best fitting curves to the data with an exponential model $Q(\tau) = e^{-\tau/\tau^*}$. Vertical thick lines are drawn in correspondence with the characteristic relaxation time τ^* obtained from the fitting model.

D. Boxplot of the expression levels of Rab5A isoform in rotating (red) and non-rotating (blue) organoids.

E. Heatmap showing the top 100 deregulated genes (top 50 up and top 50 down) in each of the 3 replicates of the rotating and non-rotating organoids.

F. Gene set enrichment analysis (GSEA) of differentially expressed genes in rotating *versus* non-rotating organoids. GSEA was performed using the Hallmarks pathway gene sets in the GSEA Molecular Signatures Database. Moderated t-statistic was used to rank the genes. Reported are significantly enriched pathways (P-value < 0.05; number of random genes with the same or more extreme ES value divided by the total number of generated gene sets) with the color of the outline of the bar corresponding to the BH-adjusted P-value.

G. GSEA Enrichment plot of differentially expressed genes in in rotating *versus* non-rotating organoids using the Hallmarks cytosolic DNA sensing pathway in the GSEA Molecular Signatures Database. The green curve corresponds to the ES (enrichment score) curve, which is the running sum of the weighted enrichment score obtained from GSEA software, while the normalized enrichment score (NES) and the corresponding P-value are reported within the graph.

H. Quantitative changes in the expression of the INF-related DNA damage resistance signature genes in rotating *versus* non-rotating organoids. The log2Fold Change is plotted on the x-axis and the significance (Wald test p value) is defined by the color code of the outline.

I. Transcription factor enrichment analysis for overlap between the input set of differentially expressed genes in rotating *versus* non-rotating organoids and entries of the ChEA and ENCODE databases. Reported in the bars is the P-value (combination of Fisher's exact test and deviation from expected rank for random input gene-set).

Figure S11

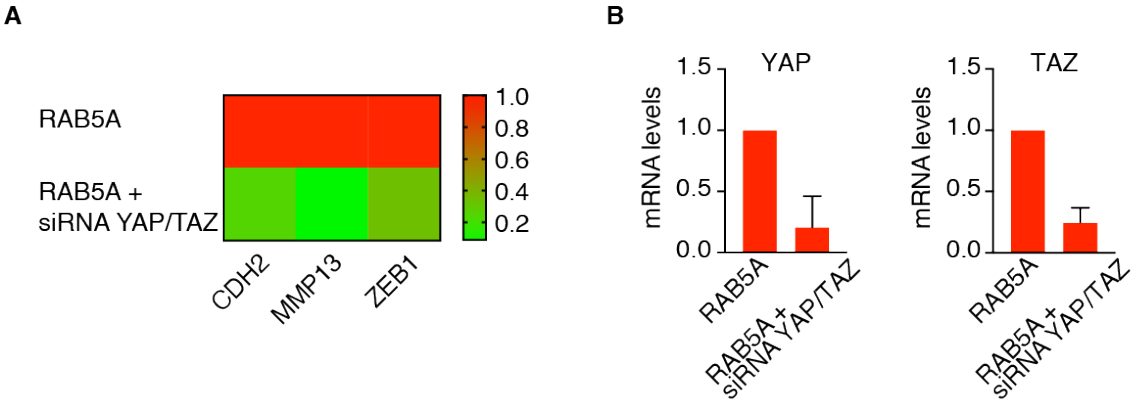

Figure S11. RAB5A induction of selected mesenchymal gene is YAP1/TAZ-dependent in fluidized MCF10.DCIS.com monolayers

A. Heatmap representing color-coded expression levels of differentially expressed EMT genes in RAB5A-expressing MCF10.DCIS.com monolayers simultaneously silenced for YAP and TAZ. The data are the ratio between the level of gene expression in each of the conditions tested relative to those of mock-treated (using scramble oligos) RAB5A-expressing cells. The mean ± s.d. (at least n = 3 independent experiments) and P values, each-pair Student's t-test (siRNA versus RAB5A-expressing cells) are reported in Table Figure S10A.

B. Box plot of the mRNA expression levels of YAP and TAZ determined by qRT-PCR in RAB5A-expressing MCF10.DCIS.com monolayer over control cells silenced with the indicated oligos. Data are expressed as mean ± s.d. (n = 3 independent experiments). Values were normalized to the controls of each experiment.

Tables S1 to S7-Raw data and statistics of the value used in the heatmaps

Table S1.

Relative expression levels of CytoDR genes presented as in the heatmap shown in Fig. 2A and statistics. In yellow are the relative expression levels of differentially expressed CytoDR genes in RAB5A-MCF10.DCIS.com monolayers silenced for the indicated genes with respect to monolayers treated with scrambled oligos. In orange, are the mean, s.d., and t-test.

	IFI27	IFI44	IFI44L	IFI6	IFIT1	IFIT3	ISG15	OASL	
RAB5A+scrambled oligos	1.00	1.00	1.00	1.00	1.00	1.00	1.00	1.00	Values of the heatmap reported in Fig 2A.
RAB5A + siRNA cGAS	0.29	0.13	0.11	0.18	0.15	0.18	0.13	0.26	Data are expressed as mean of the independent experiments reported below
RAB5 + siRNA STING	0.15	0.20	0.09	0.29	0.20	0.21	0.11	0.15	
RAB5A + siRNA IRF3	0.32	0.16	0.15	0.17	0.13	0.16	0.11	0.12	

	IFI27	IFI44	IFI44L	IFI6	IFIT1	IFIT3	ISG15	OASL	Raw data of all experimental conditions
RAB5A+scrambled oligos	1	1	1	1	1	1	1	1	
RAB5A + siRNA cGAS_1	0.42	0.26	0.19	0.42	0.38	0.47	0.22	0.63	
RAB5A + siRNA cGAS_2	0.08	0.09	0.06	0.05	0.03	0.03	0.06	0.05	
RAB5A + siRNA cGAS_3	0.36	0.05	0.07	0.07	0.04	0.04	0.11	0.11	
mean	0.286666667	0.133333333	0.106666667	0.18	0.15	0.18	0.13	0.263333333	
st dev	0.181475435	0.111504858	0.072341781	0.20808652	0.199248588	0.251197134	0.081853528	0.318956632	
t-test	0.002432164	0.000176143	2.82559E-05	0.002409363	0.001788796	0.004821337	5.12255E-05	0.016125146	

	IFI27	IFI44	IFI44L	IFI6	IFIT1	IFIT3	ISG15	OASL
RAB5A+scrambled oligos	1	1	1	1	1	1	1	1
RAB5 + siRNA STING_1				0.66	0.28		0.17	0.23
RAB5 + siRNA STING_2	0.22	0.4	0.25	0.42	0.38	0.44	0.18	0.33
RAB5 + siRNA STING_3	0.23				0.29	0.37	0.15	0.08
RAB5 + siRNA STING_4	0.07	0.15	0.02	0.06	0.03	0.02	0.03	0.08
RAB5 + siRNA STING_5	0.06	0.06	0.01	0.01	0.01	0.01	0.01	0.02
mean	0.145	0.203333333	0.093333333	0.2875	0.198	0.21	0.108	0.148
st dev	0.092556289	0.176162803	0.135769412	0.308261253	0.167242339	0.227009545	0.081363382	0.127945301
t-test	1.62141E-06	0.001434444	0.000319146	0.003605135	5.0291E-06	0.000436829	8.18791E-09	4.07925E-07

	IFI27	IFI44	IFI44L	IFI6	IFIT1	IFIT3	ISG15	OASL
RAB5A+scrambled oligos	1	1	1	1	1	1	1	1
RAB5A + siRNA IRF3_1					0.19		0.2	0.18
RAB5A + siRNA IRF3_2	0.44	0.3	0.4	0.45	0.13	0.12	0.19	0.25
RAB5A + siRNA IRF3_3	0.56				0.33	0.5		0.1
RAB5A + siRNA IRF3_4	0.11	0.05	0.03	0.02	0.01	0.005	0.02	0.05
RAB5A + siRNA IRF3_5	0.18	0.13	0.03	0.03	0.01	0.003	0.04	0.03
mean	0.3225	0.16	0.153333333	0.166666667	0.134	0.157	0.1125	0.122
st dev	0.212661703	0.127671453	0.2136196	0.245424802	0.134461891	0.235115574	0.095699181	0.092032603
t-test	0.000702084	0.000338216	0.002358058	0.004177477	5.28198E-07	0.000371414	1.58433E-06	2.45282E-08

Table S2.

Relative expression levels of CytoDR genes presented as in the heatmap shown in Fig. 2B and statistics. In yellow, are the relative expression levels of differentially expressed CytoDR genes in RAB5A-MCF10.DCIS.com monolayers treated with the indicated small molecules: cGAS inhibitor, RU.521, the STING antagonist, H-151, or the TBK1/IKK inhibitor, MRT67307. The data are the ratio between the level of gene expression in each of the conditions tested relative to vehicle-treated RAB5A-expressing cells. In orange are the mean, s.d., and t-test.

	IFI27	IFI44	IFI44L	IFI6	IFIT1	IFIT3	ISG15	OASL	
RAB5A+vehicle	1	1	1	1	1	1	1	1	Values of the heatmap reported in Fig 2B.
RAB5A + RU.521	0.0345	0.134	0.06625	0.065	0.07733333	0.0525	0.1059	0.08266667	Data are expressed as mean of the independent experiments reported below
RAB5A + H-151	0.35	0.4925	0.38	0.35	0.6	0.3375	0.305	0.4075	
RAB5A + MRT67307	0.17	0.30666667	0.27	0.20333333	0.41	0.10533333	0.167	0.22466667	

	IFI27	IFI44	IFI44L	IFI6	IFIT1	IFIT3	ISG15	OASL	Raw data of all experimental condition
RU.521_1	0.01	0.011	0.06		0.039	0.026		0.016	
RU.521_2	0.09	0.4	0.17	0.1	0.19	0.16	0.16	0.097	
RU.521_3	0.005	0.05	0.03	0.009	0.021	0.006	0.005	0.002	
RU.521_4	0.033	0.075	0.005	0.007	0.001	0.018	0.0085	0.001	
RU.521_5				0.009	0.013		0.006	0.03	
RU.521_6				0.2	0.2		0.35	0.35	
mean	0.0345	0.134	0.06625	0.065	0.077333333	0.0525	0.1059	0.082666667	
st dev	0.038957242	0.179278182	0.07272952	0.085273091	0.092031879	0.07213644	0.15178867	0.135696229	
t-test	1.80823E-05	0.002354544	0.00012956	1.64215E-05	2.08789E-06	0.00012102	0.00019192	1.46658E-05	

	IFI27	IFI44	IFI44L	IFI6	IFIT1	IFIT3	ISG15	OASL
H-151_1	0.49	0.5	0.61	0.62	0.4	0.34	0.42	0.39
H-151_2	0.23	0.46	0.49	0.3	1.4	0.67	0.18	0.32
H-151_3	0.34	0.5	0.18	0.22	0.31	0.2	0.29	0.28
H-151_4	0.34	0.51	0.24	0.26	0.29	0.14	0.33	0.64
mean	0.35	0.4925	0.38	0.35	0.6	0.3375	0.305	0.4075
st dev	0.106770783	0.022173558	0.203797285	0.18293897	0.535474867	0.236977495	0.099498744	0.161529151
t-test	0.001192754	2.29527E-05	0.008914612	0.005733683	0.232028772	0.011299627	0.000794192	0.005233051

	IFI27	IFI44	IFI44L	IFI6	IFIT1	IFIT3	ISG15	OASL
MRT67307_1	0.46	0.47	0.38	0.29	0.2	0.16	0.33	0.41
MRT67307_2	0.03	0.25	0.39	0.25	1	0.13	0.14	0.24
MRT67307_3	0.02	0.2	0.04	0.07	0.03	0.026	0.031	0.024
mean	0.17	0.306666667	0.27	0.203333333	0.41	0.105333333	0.167	0.224666667
st dev	0.251197134	0.143643076	0.199248588	0.117189306	0.517976833	0.070323064	0.151317547	0.193456283
t-test	0.029201032	0.014007594	0.023944375	0.007135649	0.187243523	0.002053112	0.010821143	0.020127931

.

Table S3.

Relative expression levels of CytoDR genes presented as in the heatmap shown in Fig. 2C and statistics. In yellow, are the relative expression levels of differentially expressed CytoDR genes in RAB5A-MCF10.DCIS.com monolayers silenced for the indicated genes with respect to monolayers treated with scrambled oligos. In orange, are the mean, s.d., and t-test.

	IFI27	IFI44	IFI44L	IFI6	IFIT1	IFIT3	ISG15	OASL	
RAB5A+scrambled oligos	1	1	1	1	1	1	1	1	Values of the heatmap reported in Fig 2C.
RAB5A + siRNA IRF9	0.12766667	0.17	0.0475	0.126	0.0828	0.13133333	0.07828571	0.115	Data are expressed as mean of the independent experiments reported below
RAB5A + siRNA STAT 1/2	0.04	0.1025	0.0206	0.121	0.045625	0.09116667	0.031875	0.04125	

	IFI27	IFI44	IFI44L	IFI6	IFIT1	IFIT3	ISG15	OASL	
siRNA IRF9_1				0.23	0.05		0.07	0.05	Raw data of all experimental
siRNA IRF9_2	0.096	0.24	0.11	0.26	0.08	0.13	0.08	0.43	
siRNA IRF9_3	0.23				0.28	0.36	0.15	0.08	
siRNA IRF9_4	0.36					0.09	0.08		
siRNA IRF9_5	0.01	0.35	0.06	0.12		0.2	0.15	0.07	
siRNA IRF9_6	0.03	0.03	0.01	0.01	0.003	0.003	0.008	0.03	
siRNA IRF9_7	0.04	0.06	0.01	0.01	0.001	0.005	0.01	0.03	
mean	0.12766667	0.17	0.0475	0.126	0.0828	0.13133333	0.07828571	0.115	
st dev	0.13894123	0.15165751	0.04787136	0.11802542	0.11514209	0.10402578	0.05768222	0.15565989	
t-test	2.1096E-05	0.00163245	3.4916E-05	7.7908E-05	5.8374E-05	1.8707E-05	1.1718E-08	3.4308E-05	

	IFI27	IFI44	IFI44L	IFI6	IFIT1	IFIT3	ISG15	OASL	
siRNA STAT1/2_1				0.42	0.09		0.07	0.04	
siRNA STAT1/2_2				0.1	0.02		0.02	0.04	
siRNA STAT1/2_3	0.04	0.15	0.02	0.08	0.03	0.11	0.03	0.16	
siRNA STAT1/2_4	0.13				0.14	0.27	0.001	0.02	
siRNA STAT1/2_5	0.01		0.05		0.02	0.002	0.008	0.03	
siRNA STAT1/2_6	0.01	0.21	0.03		0.06	0.15	0.11	0.02	
siRNA STAT1/2_7	0.02	0.02	0.002	0.002	0.002	0.005	0.006	0.01	
siRNA STAT1/2_8	0.03	0.03	0.001	0.003	0.003	0.01	0.01	0.01	
mean	0.04	0.1025	0.0206	0.121	0.045625	0.09116667	0.031875	0.04125	
st dev	0.04560702	0.09287088	0.02051341	0.17292195	0.04834382	0.10748101	0.03849467	0.0494072	
t-test	5.1878E-08	0.00030251	4.616E-08	0.00034164	1.5498E-10	4.8571E-06	2.8535E-11	1.7475E-10	

Table S4.

Relative expression levels of CytoDR genes presented as in the heatmap shown in Fig. S3A and statistics. In yellow are the relative expression levels of differentially expressed CytoDR genes in RAB5A-expressing MCF10.DCIS.com monolayers treated with the indicated small molecules. The data are the ratio between the level of gene expression in each of the conditions tested relative to vehicle-treated RAB5A-expressing cells. In orange are the mean, s.d., and t-test.

	IFI27	IFI44	IFI44L	IFI6	IFIT1	IFIT3	ISG15	OASL	
RAB5A+vehicle	1	1	1	1	1	1	1	1	Values of the heatmap reported in Fig S3A.
RAB5A + Dynasore	0.12	0.176666667	0.173333333	0.123333333	0.126666667	0.093333333	0.126666667	0.092	Data are expressed as mean of the independent experiments reported below
RAB5A + PD0325901	0.403333333	0.133333333	0.136666667	0.286666667	0.23	0.813333333	0.283333333	0.44	

	IFI27	IFI44	IFI44L	IFI6	IFIT1	IFIT3	ISG15	OASL	Raw data of all experimental conditions
Dynasore_1	0.25	0.4	0.46	0.32	0.34	0.24	0.34	0.26	
Dynasore_2	0.09	0.09	0.04	0.03	0.03	0.03	0.03	0.01	
Dynasore_3	0.02	0.04	0.02	0.02	0.01	0.01	0.01	0.006	
mean	0.12	0.176666667	0.173333333	0.123333333	0.126666667	0.093333333	0.126666667	0.092	
st dev	0.117898261	0.195021366	0.248461935	0.170391706	0.185022521	0.127410099	0.185022521	0.145506014	
t-test	0.00592996	0.018193338	0.028816622	0.01235938	0.01463365	0.006518215	0.01463365	0.008451542	

	IFI27	IFI44	IFI44L	IFI6	IFIT1	IFIT3	ISG15	OASL
PD0325901_1	0.31	0.16	0.12	0.27	0.2	1	0.35	0.41
PD0325901_2	0.42	0.11	0.16	0.33	0.35	0.84	0.32	0.43
PD0325901_3	0.48	0.13	0.13	0.26	0.14	0.6	0.18	0.48
mean	0.403333333	0.133333333	0.136666667	0.286666667	0.23	0.813333333	0.283333333	0.44
st dev	0.086216781	0.025166115	0.02081666	0.037859389	0.108166538	0.201328918	0.090737717	0.036055513
t-test	0.006888006	0.000280947	0.000193739	0.000937626	0.006513639	0.249521226	0.005300978	0.001378945

Table S5.

Relative expression levels of CytoDR genes presented as in the heatmap shown in Fig. S3A and statistics. In yellow, are the relative expression levels of differentially expressed CytoDR genes in RAB5A-MCF10.DCIS.com monolayers treated with the indicated small molecules. The data are the ratio between the level of gene expression in each of the conditions tested relative to vehicle-treated RAB5A-expressing cells. In orange, are the mean, s.d., and t-test.

	IFI27	IFI44	IFI44L	IFI6	IFIT1	IFIT3	ISG15	OASL	
RAB5A+vehicle	1	1	1	1	1	1	1	1	Values of the heatmap reported in Fig S5E.
RAB5A + MK886	0.826666667	0.703333333	0.626666667	0.76	0.503333333	0.403333333	0.626666667	0.643333333	Data are expressed as mean of the independent experiments reported below
RAB5A + Blebbistatin	1.11333333	0.6	0.88333333	0.6425	0.79	0.63666667	0.51	0.77	

	IFI27	IFI44	IFI44L	IFI6	IFIT1	IFIT3	ISG15	OASL	Raw data of all experimental conditions
MK886_1	0.61	0.7	0.6	1	0.67	0.51	0.68	0.82	
MK886_2	0.72	0.83	0.7	0.7	0.28	0.21	0.54	0.51	
MK886_3	1.15	0.58	0.58	0.58	0.56	0.49	0.66	0.6	
mean	0.826666667	0.703333333	0.626666667	0.76	0.503333333	0.403333333	0.626666667	0.643333333	
st dev	0.285365263	0.125033329	0.064291005	0.216333077	0.201080415	0.167729942	0.075718778	0.159478316	
t-test	0.403126283	0.054421354	0.009741002	0.194612734	0.050531604	0.02534414	0.013436011	0.060644258	

	IFI27	IFI44	IFI44L	IFI6	IFIT1	IFIT3	ISG15	OASL
Blebbistatin_1	1.1	0.74	0.65	0.41	0.69	0.72	0.49	0.25
Blebbistatin_2	1.5	0.56	1.15	0.86	0.81	0.33	0.45	0.13
Blebbistatin_3	0.74	0.5	0.85	1	0.54	0.86	0.31	1.3
Blebbistatin_4				0.3			0.79	1.4
mean	1.113333333	0.6	0.883333333	0.6425	0.68	0.636666667	0.51	0.77
st dev	0.380175398	0.12489996	0.251661148	0.339840649	0.135277493	0.274651294	0.201990099	0.672755528
t-test	0.657037731	0.030996834	0.506258069	0.126093056	0.054726094	0.149034587	0.016712932	0.543208296

Table S6.

Relative expression levels of CytoDR genes presented as in the heatmap shown in Fig. S6E and statistics. In yellow, are the relative expression levels of differentially expressed CytoDR genes in RAB5A-MCF10.DCIS.com monolayers treated with the indicated small molecules. The data are the ratio between the level of gene expression in each of the conditions tested relative to vehicle-treated RAB5A-expressing cells. In orange, are the mean, s.d., and t-test.

	IFI27	IFI44	IFI44L	IFI6	IFIT1	IFIT3	ISG15	OASL	
RAB5A+vehicle	1	1	1	1	1	1	1	1	Values of the heatmap reported in Fig S6E.
RAB5A + Latrunculin	0.515	1.07	0.505	0.62	1.09	0.66	0.58	0.535	Data are expressed as mean of the independent experiments reported below
	IFI27	IFI44	IFI44L	IFI6	IFIT1	IFIT3	ISG15	OASL	Raw data of all experimental conditions
Latrunculin_1	0.6	1.46	0.44	0.76	1	0.54	0.76	0.66	
Latrunculin_2	0.43	0.68	0.57	0.48	1.18	0.78	0.4	0.41	
mean	0.515	1.07	0.505	0.62	1.09	0.66	0.58	0.535	
st dev	0.120208153	0.551543289	0.091923882	0.197989899	0.127279221	0.169705627	0.254558441	0.176776695	
t-test	0.110450811	0.886938768	0.083120958	0.22472066	0.5	0.216000387	0.257762117	0.167182131	

Table S7.

Relative expression levels of CytoDR genes presented as in the heatmap shown in Fig. S10E and statistics. In yellow, are the relative expression levels of differentially expressed CytoDR genes in RAB5A-MCF10.DCIS.com monolayers silenced for the indicated genes with respect to monolayers treated with scrambled oligos. In orange, are the mean, s.d., and t-test.

	CDH2	MMP13	ZEB1	
RAB5A+scrambled oligos	1	1	1	Values of the heatmap reported in Fig S10A.
RAB5A + siRNA YAP/TAZ	0.245	0.09	0.33	Data are expressed as mean of the independent experiments reported below

	CDH2	MMP13	ZEB1	Raw data of all experimental conditions
RAB5A+scrambled oligos	1	1	1	
RAB5A + siRNA YAP/TAZ_1	0.41	0.17	0.36	
RAB5A + siRNA YAP/TAZ_2	0.42		0.32	
RAB5A + siRNA YAP/TAZ_3	0.09	0.07	0.31	
RAB5A + siRNA YAP/TAZ_4	0.06	0.03	0.32	
mean	0.245	0.09	0.3275	
st dev	0.19672316	0.07211103	0.02217356	
t-test	0.00459395	0.0020866	9.8715E-06	

References

85. Palamidessi, A. *et al.* Unjamming overcomes kinetic and proliferation arrest in terminally differentiated cells and promotes collective motility of carcinoma. *Nat Mater* **18**, 1252-1263 (2019).
86. Sachs, N. *et al.* A Living Biobank of Breast Cancer Organoids Captures Disease Heterogeneity. *Cell* **172**, 373-386 e310 (2018).
87. Dobin, A. *et al.* STAR: ultrafast universal RNA-seq aligner. *Bioinformatics* **29**, 15-21 (2013).
88. Love, M.I., Huber, W. & Anders, S. Moderated estimation of fold change and dispersion for RNA-seq data with DESeq2. *Genome Biol* **15**, 550 (2014).
89. Sergushichev, A.A. An algorithm for fast preranked gene set enrichment analysis using cumulative statistic calculation. *bioRxiv*, 060012 (2016).
90. Della Chiara, G. *et al.* Epigenomic landscape of human colorectal cancer unveils an aberrant core of pan-cancer enhancers orchestrated by YAP/TAZ. *Nat Commun* **12**, 2340 (2021).
91. He, D.C., Nickerson, J.A. & Penman, S. Core filaments of the nuclear matrix. *J Cell Biol* **110**, 569-580 (1990).
92. Bolger, A.M., Lohse, M. & Usadel, B. Trimmomatic: a flexible trimmer for Illumina sequence data. *Bioinformatics* **30**, 2114-2120 (2014).
93. Li, H. & Durbin, R. Fast and accurate short read alignment with Burrows-Wheeler transform. *Bioinformatics* **25**, 1754-1760 (2009).
94. Li, H. *et al.* The Sequence Alignment/Map format and SAMtools. *Bioinformatics* **25**, 2078-2079 (2009).
95. Kharchenko, P.V., Tolstorukov, M.Y. & Park, P.J. Design and analysis of ChIP-seq experiments for DNA-binding proteins. *Nat Biotechnol* **26**, 1351-1359 (2008).
96. Hahne, F. & Ivanek, R. Visualizing Genomic Data Using Gviz and Bioconductor. *Methods Mol Biol* **1418**, 335-351 (2016).
97. Ramirez, F. *et al.* deepTools2: a next generation web server for deep-sequencing data analysis. *Nucleic Acids Res* **44**, W160-165 (2016).
98. Schmidt, U., Weigert, M., Broaddus, C. & Myers, G. 265-273 (Springer International Publishing, Cham; 2018).
99. Hu, M. *et al.* Regulation of in situ to invasive breast carcinoma transition. *Cancer cell* **13**, 394-406 (2008).
100. Gioia, U. *et al.* Pharmacological boost of DNA damage response and repair by enhanced biogenesis of DNA damage response RNAs. *Sci Rep* **9**, 6460 (2019).
101. Gyori, B.M., Venkatachalam, G., Thiagarajan, P., Hsu, D. & ClÈment, M. OpenComet: An automated tool for comet assay image analysis. *Redox Biology* **2**, 457 - 465 (2014).
102. Schneider, C.A., Rasband, W.S. & Eliceiri, K.W. NIH Image to ImageJ: 25 years of image analysis. *Nat Methods* **9**, 671-675 (2012).
103. Schindelin, J. *et al.* Fiji: an open-source platform for biological-image analysis. *Nat Methods* **9**, 676-682 (2012).
104. Wahlby, C., Lindblad, J., Vondrus, M., Bengtsson, E. & Bjorkesten, L. Algorithms for cytoplasm segmentation of fluorescence labelled cells. *Anal Cell Pathol* **24**, 101-111 (2002).
105. Lim, J.S. *Two-dimensional signal and image processing*. (Prentice Hall, Englewood Cliffs, N.J.; 1990).
106. Meyer, F. Topographic distance and watershed lines. *Signal Processing* **38**, 113-125 (1994).
107. Jolliffe, I.T. & Cadima, J. Principal component analysis: a review and recent developments. *Philos Trans A Math Phys Eng Sci* **374**, 20150202 (2016).
108. Crocker, J.C. & Grier, D.G. Methods of Digital Video Microscopy for Colloidal Studies. *Journal of Colloid and Interface Science* **179**, 298-310 (1996).

109. Thielicke, W. & Sonntag, R. Particle Image Velocimetry for MATLAB: Accuracy and enhanced algorithms in PIVlab. *Journal of Open Research Software* **9(1),** (2021).
110. Beznoussenko, G.V. *et al.* Transport of soluble proteins through the Golgi occurs by diffusion via continuities across cisternae. *Elife* **3** (2014).
111. Beznoussenko, G.V., Ragnini-Wilson, A., Wilson, C. & Mironov, A.A. Three-dimensional and immune electron microscopic analysis of the secretory pathway in Saccharomyces cerevisiae. *Histochem Cell Biol* **146**, 515-527 (2016).
112. Beznoussenko, G.V. & Mironov, A.A. Correlative video-light-electron microscopy of mobile organelles. *Methods Mol Biol* **1270**, 321-346 (2015).
113. Koeberle, A. *et al.* MK-886, an inhibitor of the 5-lipoxygenase-activating protein, inhibits cyclooxygenase-1 activity and suppresses platelet aggregation. *Eur J Pharmacol* **608**, 84-90 (2009).

Other Supplementary Materials for this manuscript include the following:

Movies S1 to S9

Movie S1.
Control (CTR) or RAB5A-MCF10.DCIS.com monolayers expressing mCherry-H2B treated with hypotonic solution were monitored by fluorescence time-lapse microscopy over a 48 hours period. Pictures were taken every 15 minutes (see Fig. S2D). Scale bar, 10 μm.

Movie S2.
Control or RAB5-expressing HaCat monolayers were seeded at a jamming density, serum starved for 2 days, doxycycline-treated and monitored by time-lapse phase-contrast microscopy in the presence or the absence of EGF (100 ng/ml). Frames were acquired with every 5 min over a period of 48 hours (see Fig. S3C-E). Scale bar, 100 μm.

Movie S3.
RAB5A promotes cell fluctuations in confluent monolayer. Space and time cell fluctuations were monitored in MCF-10A cells stably expressing EGFP-E-cadherin by fluorescence time-lapse microscopy over a 24 hours period. Pictures were taken every 5 min and random pseudo colors are selected for different cell identities (see Fig. 2E-G). Scale bar, 20 μm.

Movie S4.
Nuclear segmentation and tracking of nuclear shape changes. Control and RAB5A-MCF10A expressing mCherry-H2B were monitored by fluorescence time-lapse microscopy over a 24 hours period. Pictures were taken every 10 min. The upper panels show randomly picked cell nuclei in which the continuous green lines with different shades of green represent the corresponding fluctuating profiles of nuclear contours obtained *via* nuclear segmentations (see Fig. 2H-I). In the bottom magnified panels, the red lines indicate the representative fluctuating profiles of nuclear contours of control and RAB5A-MCF10A cells in a monolayer. Scale bar, 4 μm.

Movie S5.
Control MCF10.DCIS.com monolayers expressing mCherry-H2B were transfected with EGFP-cGAS. After defining the region of interest, pre bleach images were collected for 30 seconds at a rate of 5 seconds per timepoint. Photobleaching was performed using UltraVIEW PK Device as a bleaching device on a small spot over the nuclear envelope. Images were captured for 300 seconds at a rate of 5 seconds per timepoint (see Fig. S5A). Scale bar, 8 μm.

Movie S6.
Control and RAB5A-MCF10.DCIS.com monolayers expressing EGFP-3NLS were seeded at jamming density. After treatment with doxycycline to induce transgene expression, monolayers were monitored by fluorescence time-lapse microscopy over a 30 hours period. Picture were taken every 15 min. The leakage of EGFP-3NLS into the cytoplasm is indicative of NE ruptures (see Fig. 3D-E) Scale bar, 15 μm.

Movie S7.
Living breast cancer organoids labelled with NucLight and embedded into Matrigel were monitored by fluorescence time-lapse microscopy over a period of 24 hours. Pictures were taken every 15 min. (see Fig S10A-C). Scale Bar, 8 μm.

Movie S8.
3D rendering of five living breast cancer organoids labelled with NucLight and embedded into Matrigel were monitored by fluorescence time-lapse microscopy over a period of 24 hours. Pictures were taken every 15 min. The size of each box along the x- and y-directions corresponds to 200 μm. In the bottom panels, thin blue, orange and yellow curves are the temporal evolution of the x, y and z components of the angular velocity associated with the rotation of the organoid depicted in the box above each panel, respectively. Thick black curves represent the angular speed, *i.e.,* the modulus of the angular velocity. Organoids are categorized as "rotating" if their average angular speed is larger than $0.03\,\mathrm{cycles/h}$, as "non rotating" otherwise (see Fig S10A-B).

Movie S9.
A semi-automated image analysis pipeline to quantify the location of the γH2AX expressing cells in the tumoral ductaladenocarcinoma regions. A deep learning based nuclear segmentation (Stardist)[98] was employed to segment individual nuclei and identified the centroid positions of each nuclei in the image frame. A semi-automated analysis was used to identify the location of whole area, the core region and the outer margin of the ductaladenocarcinoma. An automated histogram-based thresholding in each frame to identify regions with high expression of γH2AX signal, above the threshold applied. Isolated small spots were removed as noise. Nuclei that display either a positive or weak/absent (below the arbitrary established threshold levels) γH2AX signal were identified. For each case, we quantified the total number of nuclei, the number of nuclei with strongly positive or weak/no γH2AX signal in the tumor core, tumor surface and in the whole tumoral areas and computed the percentage of nuclei with strongly positive γH2AX signal in the core region, tumor front regions and in the whole tumor region over 9 independent cases (see Materials and Methods for details).

RNA-seq data
RNA-seq data of MCF10A and MCF10.DCIS.com cells and of organoids are being submitted respectively to Gene Expression Omnibus (GEO) and European Genome-phenome Archive (EGA) and are available upon request.